Available online at www.sciencedirect.com

ScienceDirect

Geochimica et Cosmochimica Acta 151 (2015) 150–167

Geochimica et Cosmochimica Acta

www.elsevier.com/locate/gca

Comparative microbial diversity and redox environments of black shale and stromatolite facies in the Mesoproterozoic Xiamaling Formation

Genming Luo [a,b,*], Christian Hallmann [c,d], Shucheng Xie [a], Xiaoyan Ruan [e], Roger E. Summons [b]

[a] State Key Laboratory of Biogeology and Environmental Geology, China University of Geosciences, Wuhan 430074, People's Republic of China
[b] Department of Earth, Atmospheric and Planetary Sciences, Massachusetts Institute of Technology, 77 Massachusetts Avenue E34-246, Cambridge, MA 02139, USA
[c] Max-Planck-Institute for Biogeochemistry, Jena, Germany
[d] MARUM, University of Bremen, Building IW-3, Am Biologischen Garten 2, 28359 Bremen, Germany
[e] Department of Petroleum Geology, Faculty of Earth Resources, China University of Geosciences, Wuhan, 430074, China

Received 30 September 2014; accepted in revised form 19 December 2014; available online 29 December 2014

Abstract

The composition of microbial communities and their relationship to ocean redox structure in the Precambrian are topics of continuing interest in geobiology. Our knowledge of organismic diversity and environmental conditions during this time are mostly based on fragmentary paleontological and geochemical records and might be skewed accordingly. In North China the Xiamaling Formation (~1.37 Ga) is characterized by black shales of relatively low thermal maturity (T_{max} is ~445 °C) and has been identified as a potential petroleum source rock. To date, however, the biological sources of the organic matter and the environmental conditions prevalent during the deposition of these sediments remain unclear. In this study we analyzed the hydrocarbon biomarker compositions of the Xiamaling Formation shales and a superjacent stromatolitic carbonate in order to shed light on the microbial diversity in the sedimentary environments they represent. The hydrocarbons extracted from both sediments are dominated by low-molecular-weight *n*-alkanes with a maximum at $C_{15–18}$, suggesting that bacteria and/or algae were primary biotic precursors. Our inability to detect steranes in bitumen I, and only traces of rearranged steranes in bitumen II of black shales, indicates that modern eukaryotic algae were either ecologically insignificant or not preserved due to a taphonomic bias. The high relative concentration of hopanes and diahopanes ranging from C_{27} to C_{35}, as well as monomethylalkanes, suggests that cyanobacteria may have been the dominant primary producers and could have contributed to the biologically available nitrogen pool through N_2-fixation. This observation is supported by the low nitrogen isotopic composition of the kerogens. Even though all facies zones appear to have been anoxic but not sulfidic on the basis of biomarker ratios and trace metals, subtle but distinct molecular differences are observed between the stromatolite and the black shales, which can be attributed to both, lithologically-controlled diagenetic rearrangements and differential biotic input. The discrepancy between the presence of a large UCM and high abundances of alkyl lipids on one hand, yet the absence of a stable carbon isotopic offset between lipids and kerogen, on the other, suggests that strong heterotrophic reworking might not be the sole source of the biodegraded fingerprint that is so typical for Proterozoic bitumens, and demands alternative explanations.
© 2014 Elsevier Ltd. All rights reserved.

* Corresponding author at: State Key Laboratory of Biogeology and Environmental Geology, China University of Geosciences, Wuhan 430074, People's Republic of China.
E-mail address: gmluo@mit.edu (G. Luo).

http://dx.doi.org/10.1016/j.gca.2014.12.022
0016-7037/© 2014 Elsevier Ltd. All rights reserved.

1. INTRODUCTION

Geological and geochemical records suggest that bacterial life, including sulfur-metabolizing microbes, evolved on Earth prior to ca. 3.5 Ga (billion years ago) (Shen et al., 2001; Allwood et al., 2006; Derenne et al., 2008; Ueno et al., 2008; Bontognali et al., 2012). Although the timing of the first emergence of eukaryotes is still debated (e.g., Knoll, 1992; Cavalier-Smith, 2002; Yoon et al., 2004), acanthomorph acritarchs recovered from the Roper Group in Australia testify of their presence by 1.5 Ga (Javaux et al., 2001, 2010; Knoll et al., 2006). Their rise to ecological significance however only occurred during the Middle Neoproterozoic (Knoll et al., 2006). Due to the sparse preservation of physical remains, very little is known about organismic diversity, and especially, the environmental prevalence of eukaryotic algae, in the period between these events, i.e., roughly covering the late Mesoproterozoic Era and Tonian Period. In contrast to acritarch microfossils, which evade exact taxonomic classification and which do not provide contextual environmental details, the sedimentary hydrocarbon remnants of biologically produced lipids can present a wealth of information on microbial diversity and environmental conditions during deposition and early diagenesis (e.g., Summons and Lincoln, 2012). But for the aforementioned period that lies between the first occurrence of undisputed eukaryotic microfossils (1.49 Ga, Roper Group) and the oldest detection of unambiguously syngenetic eukaryotic steranes (ca. 0.75 Ga, Chuar Group) our knowledge is currently limited to only a handful of biomarker studies that targeted rocks at 1.10 Ga (Oronto Group, USA; Imbus et al., 1988; Pratt et al., 1991), 1.11 Ga (Atar Group, Mauretania; Blumenberg et al., 2012) and 1.43 Ga (Roper Group, Australia; Dutkiewicz et al., 2003). The relevance of every additional study contributing to our understanding of Earth system evolution at this period in Earth history is thus incontestable. In addition, only few studies have evaluated the diversity of preserved hydrocarbons across different facies, a consequence of which is that we still know very little about the principle primary producers and their ecological zonation during much of the Precambrian.

Since many Precambrian rocks have seen protracted burial, tectonic movement and late-stage fluid flow, any issues concerning the indigenous nature of extracted lipid biomarkers must be resolved before they can be used to reconstruct biotic composition and sedimentary environments. Recent studies have indicated that at least some of previously published results have been affected to varying degrees by contamination (Rasmussen et al., 2008; Brocks, 2011) and specifically question any conclusions regarding the presence of steranes and first appearance of eukaryotes in the Archean (Brocks et al., 1999). Accordingly, we are in need of further studies, using suitably preserved material from a variety of Precambrian settings to enhance our understanding of microbial diversity, as well as its temporal changes, in Precambrian oceans.

Due to the enhanced preservation of organic matter on clay mineral surfaces and their low permeability to migrating fluids, black shales have been considered to be a prime target for Precambrian biomarker research (Summons et al., 1988a,b; Pratt et al., 1991; Brocks et al., 2005; Eigenbrode et al., 2008; Waldbauer et al., 2009; Blumenberg et al., 2012). For example, Brocks et al. (2005) found abundant hydrocarbon biomarkers derived from green sulfur bacteria, purple sulfur bacteria and aerobic methane oxidizing bacteria in black shales of the ~1.64-Ga-old Barney Creek Formation in northern Australia, whose molecular inventory has been widely accepted as containing the oldest convincing indigenous biomarkers. In northern China (Fig. 1), the Mesoproterozoic Xiamaling Formation is characterized by a high TOC content of black

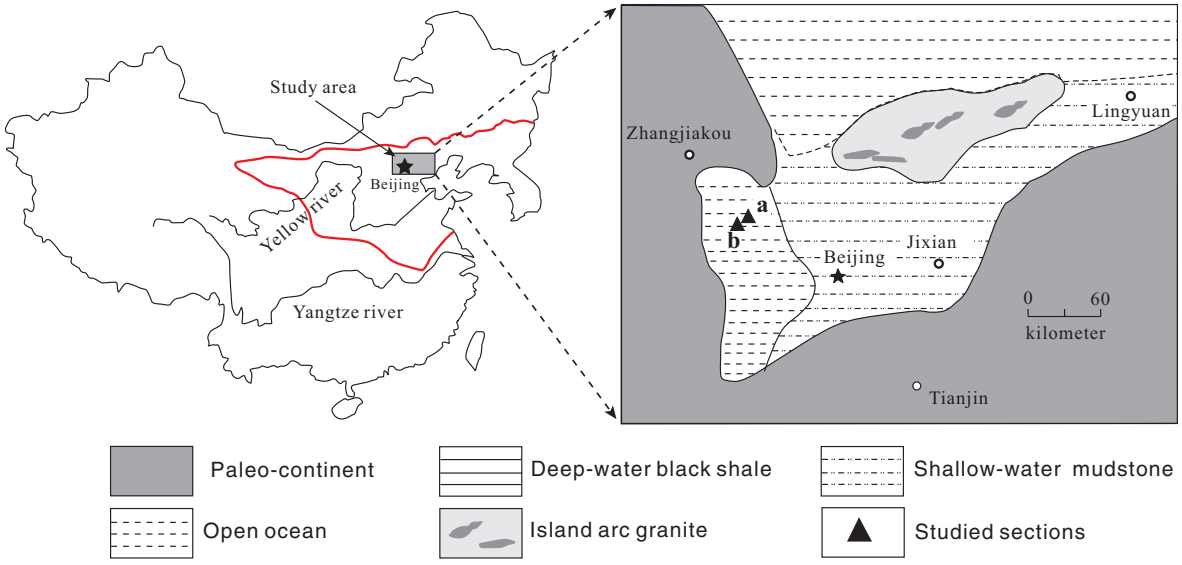

Fig. 1. Paleogeography of the North China Craton (NCC) outlined by the red line during the deposition of the Xiamaling Formation (modified after Qiao et al. (2007) and locations of the studied sections. (For interpretation of the references to colour in this figure legend, the reader is referred to the web version of this article.)

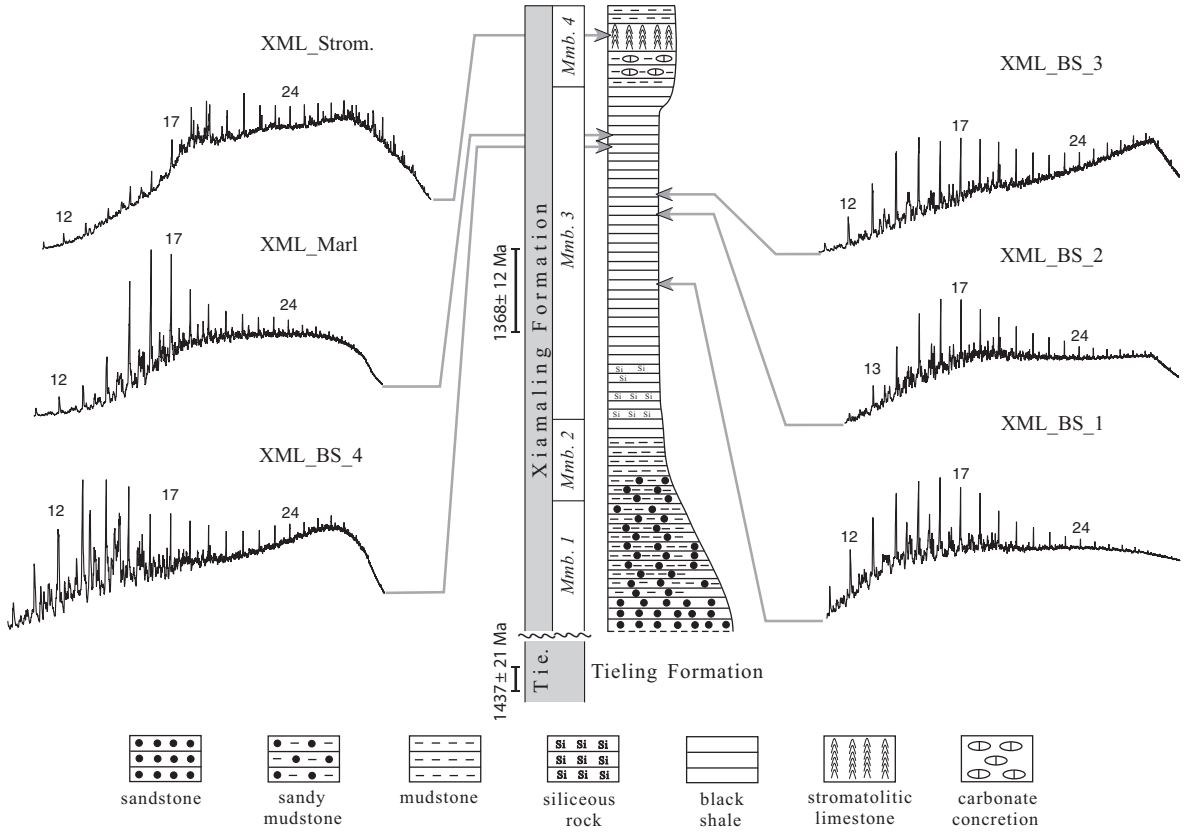

Fig. 2. Composite lithological and stratigraphic column of the Xiamaling Formation in Zhangjiakou city, Hebei Province and TIC of samples analyzed in this study. The numbers above peaks indicate the carbon number of the *n*-alkanes.

shales of its third stratigraphic member (Fig. 2). Considering the relatively low thermal maturity of these black shales (see discussion further below), they were identified as potential oil source rocks (Xie et al., 2013). The overlying fourth member of the Xiamaling Formation consists of grey mudstone and contains abundant stromatolites. In this study we have analyzed the hydrocarbon composition of black shales and carbonate in the Xiamaling Formation in order to unravel the biotic precursors of the organic matter, sedimentary environments and ecological zonation in the aquatic environment that accumulated the Xiamaling Fm. In addition to the hydrocarbon data, we have analyzed the stable nitrogen isotopic composition of kerogens, the stable carbon isotopic compositions of kerogen and individual *n*-alkanes, as well as the trace element composition of the black shales to enhance our understanding the sedimentary environment that prevailed during the deposition of these sediments.

2. MATERIALS AND METHODS

2.1. Geological setting and samples

The Xiamaling Formation was deposited in the Yanshan–Taihangshan aulacogen—an intracontinental rift basin in the center of the North China Craton (NCC) (Lu et al., 2008). Recent U–Pb dating with single grain zircons from bentonites in the Xiamaling Formation yielded an age of 1368 ± 12 Ma (Gao et al., 2008; Su et al., 2008), placing the Xiamaling Formation in the middle Mesoproterozoic—a significant revision from previously assumed Neoproterozoic age assignments. A minimum age is provided by intruding mafic sills, dated to 1320 ± 6 Ma with zircons and baddeleyites (Li et al., 2009), while upper age estimates come from the underlying Tieling Formation, which has been dated to 1437 ± 21 Ma (Su et al., 2010). In ascending order, the Xiamaling Formation can be divided into four stratigraphic members. Member 1 consists mainly of fine ferruginous sandstone, sandy mudstone and mudstone, with a weathering crust of cherty breccia and ferruginous sandstone at its base. Member 2 is dominated by amaranth and green mudstone with marly concretions and a bed of glauconitic sandstone at its base. Member 3, being the thickest (~250 m), is characterized by black shales with siliceous rocks in its lower part and several beds of bentonites (Su et al., 2010), while Member 4 contains grey and dark grey mudstone, including carbonate concretions, and stromatolitic carbonate units. The lower two members represent a retrograde sequence deposited as a consequence of sea-level rise (Wang and Li, 1993; Qiao et al., 2007) and were deposited in supratidal to intertidal (Member 1) and subtidal (Member 2) zones (Wang and Li, 1993). The third, black shale dominated member was principally deposited in basinal deep-water environments, while the carbonate dominated deposits of Member 4 can be attributed to environments of the upper subtidal to supratidal zones (Wang

Table 1
Bulk geochemistry of the samples analyzed in this study. A dash (–) indicates no analysis.

Sample No.	Lithology	Member	TOC (wt.%)	T_{max} (°C)	HI	$\delta^{13}C_{org}$ (‰ VPDB)	$\delta^{15}N_{org}$ (‰Air)	Mo (ppm)	V (ppm)	Sc (ppm)	Cr (ppm)	Th (ppm)	U (ppm)	Ni (ppm)
XML_strom.	Carbonate	4th member	0.12	439	150	–	–	–	–	–	–	–	–	–
XML_marl	Marl	3rd member	0.19	–	–	−33.1	1.9	0.82	117	15.1	17.2	5.81	3.55	18.9
XML_BS_4	Black shale	3rd member	3.37	–	–	−34.1	2.4	9.25	224	8.77	36.0	9.63	4.86	82.8
XML_BS_3	Black shale	3rd member	2.88	446	346	−33.6	2.2	9.96	302	12.1	47.9	10.6	5.81	130
XML_BS_2	Black shale	3rd member	4.10	445	312	−32.6	2.0	13.5	249	7.21	22.0	7.24	5.99	32.7
XML_BS_1	Black shale	3rd member	1.79	437	352	−32.8	–	18.8	262	14.9	46.7	8.71	6.33	35.5

and Li, 1993). The upper part of the third member and the fourth member form a prograding sequence.

Samples analyzed in this study (Table 1) include black shales from the third member of the Xiamaling Formation that were sampled in outcrop at the Zhaojiashan section (N: 40°28′38.92″, E: 115°23′19.8″, H: 881 m) in Huailai County and stromatolitic carbonates from the fourth member of the Xiamaling Formation, collected in the Huangtugang section (N: 40°27′10.27″, E: 115°13′6.04″, H: 648 m) in Zhulu County (Fig. 1).

2.2. Experiment methods

2.2.1. Materials

Prior to workup, glassware, glass wool, silica gel and aluminum foil were baked at 500 °C for 8 h and quartz sand was baked at 850 °C for >12 h to remove organic contaminants. Activated copper, used to sequester elemental sulfur, was cleaned by ultrasonication in methanol (MeOH) and dichloromethane (DCM) three times each after activation with hydrochloric acid (HCl). All solvents (*n*-hexane, DCM and MeOH) used in sample extraction and cleaning of equipment were of high purity grade (OmniSolv, EMD Chemicals). Deionized (DI) water and HCl_{aq} used to process samples were cleaned by five consecutive liquid–liquid extraction steps with DCM in a separatory funnel.

2.2.2. Sample preparation

The procedure used in this study was adopted from Brocks et al. (2003), Sherman et al. (2007) and Hallmann et al. (2011) for Precambrian organic-lean samples and is summarized only briefly here. We obtained fresh samples from outcrop in the field. Black shales were collected from an active quarry at the Zhaojiashan section and thus were not exposed to extended surface weathering. In the laboratory the samples were divided into exterior and interior portions by cutting them into small chips. Both the exterior and interior of the samples (except for the interbedded marl within the black shale) were analyzed separately in order to test for the presence of differences in the biomarker composition and thus contamination. The small chips were ultrasonicated in MeOH and DCM for 1 min each, ground to a fine powder (<100 mesh) using a stainless-steel puck mill that was cleaned by grinding baked quartz sand multiple times and by ultra-sonication in MeOH and DCM. Between samples the puck mill was cleaned by grinding baked quartz sand for three times followed by sequential washing with tap and DI water as well as by ultrasonication in MeOH and DCM for ~5 min, respectively. Before grinding a sample, the last aliquot of baked quartz sand was processed with the clean puck mill as a procedural blank.

2.2.3. Extraction and separation

Aliquots of 10–120 g of powdered rock were extracted several times in a Dionex accelerated solvent extractor (ASE 350) using DCM and MeOH (9:1 by vol.). The free extracts (Bitumen I) were collected in large beakers (1000 mL), which were loosely covered with aluminum foil and allowed to evaporate in the fume hood to a volume of

~1 mL. Special care was taken to ensure that the extracts did not evaporate to completely. Before column chromatography, the total extracts were separated into asphaltenes and maltenes by asphaltene precipitation in an excess of hexane. The maltenes were separated into saturated, aromatic and polar fractions using silica gel (activated at 150 °C for 6 h) column chromatography by sequential elution with hexane (one half column dead-volume), DCM:hexane (1:4, two dead-volumes), DCM:hexane (1:1, two dead-volumes) and MeOH (1 dead-volume).

The extracted rock powder was demineralized in Teflon tubes that were cleaned by boiling in hydrogen peroxide and by ultrasonication in organic solvents. Carbonates were removed with DCM-extracted HCl_{aq} (6 M) and residues were neutralized with DCM-extracted ultrapure water (18 MΩ*cm). Subsequently silicates were digested with 48% aqueous hydrofluoric acid (HF), rinsed with DCM-extracted water to near neutrality and dried in an oven at 60 °C. Resulting residues were extracted five times by ultrasonication in hexane, each step lasting 30 min. The extracts were pooled, filtered (quartz sand and silica gel) and concentrated as described afore. These extracts obtained after mineral digestion are termed 'Bitumen II'.

2.2.4. Instrumental analyses

Saturated and aromatic hydrocarbon fractions were analyzed by gas chromatography with a flame ionization detector (GC-FID), and by GC coupled with mass spectrometry (GC–MS) in full scan and selective ion recording (SIM) modes on a DB-1 MS capillary column (60 m, 0.25 mm i.d., 0.25 μm film thickness). Samples, dissolved in hexane, were introduced to an Agilent 6890 N GC through a PTV injector operated in splitless mode. The GC was programmed from 70 to 300 °C at 3 °C min^{-1} with a final hold time of 30 min, and a constant flow of helium (1 mL min^{-1}) was used as the carrier gas. Ionization in the MS (Micromass Autospec Ultima mass spectrometer) was achieved at 70 eV and 250 °C and the scan range was 50–550 Da. Biomarker analyses of the saturated and aromatic fractions were conducted by metastable reaction monitoring (MRM) GC–MS on the same instrument, ramping the temperature from 60 to 150 °C at 10 °C min^{-1}, then at 3 °C min^{-1} to 315 °C, where it was held for 24 min. The ion source was operated in EI-mode at 250 °C, 70 eV ionization energy and 8 kV accelerating voltage.

2.2.5. Compound-specific stable carbon isotope measurements

The saturated hydrocarbon fraction was separated into *n*-alkanes and branched/cyclic hydrocarbons using 5 Å zeolite molecular sieve, which was activated at 150 °C for 6 h. The trapped *n*-alkanes were recovered by liquid–liquid extraction with hexane (5×) after digesting the sieve with HF_{aq} in cleaned Teflon tubes. The extracts were passed through a pipette packed with quartz sand and silica gel in order to remove any particles and HF that may have been pipetted into the vial. After drying, the carbon isotopic composition of *n*-alkanes was analyzed using a Thermo Finnigan Delta plus XP coupled to a Thermo Finnigan Trace GC (GC-irMS). The initial GC oven was set at 60 °C (held for 3 min.), ramped to 180 °C at 10 °C min^{-1}, and then to 320 °C at 4 °C min^{-1} and held for 20 min. All samples were bracketed by pulses of in house calibrated reference CO_2 gas and by commercially obtained calibrated reference CO_2 gas (Oztech). A standard mix of *n*-alkanes ('Mix A'; Arndt Schimmelmann, Indiana University) was analyzed twice a day to monitor the instrument condition. The mean value of triplicate analyses are reported here in the permil (‰) notation relative to Vienna Pee Dee belemnite (VPDB), and the standard deviation from the mean value was always better than 0.4‰.

2.2.6. Bulk organic nitrogen isotopic composition

The nitrogen isotopic composition of the organic matter in the samples was determined after decalcification using an online method. After carbonate removal, about 40–55 mg of the residue was mixed with 2 mg V_2O_5 and loaded into a clean tin cup. Tin cups were introduced by an autosampler into a FlashEA 1112 HT interfaced to a Thermo MAT 253 mass spectrometer that had an average precision better than ±0.3‰. Blanks were run between every sample, and every third sample was followed by a standard (Glycine from SIGMA, $\delta^{15}N = +10.0‰$). CO_2 generated during combustion was removed by using a Carbosorb trap, while water was trapped on anhydrous magnesium perchlorate. Isotopic data are reported in the permil (‰) notation relative to atmospheric N_2.

2.2.7. Trace elements and Rock–Eval pyrolysis

Trace elements were measured in the State Key Laboratory of Geological Processes and Mineral Resources at China University of Geosciences according to methods of Liu et al. (2008). Fresh samples were crushed to <200 mesh and dissolved with a mixture of HF and HNO_3 in Teflon bombs. The solution was analyzed by Inductively Coupled Plasma (ICP)-MS with a precision >5 wt.%. The total organic carbon content (TOC) and thermal maturity of the samples (T_{max}, i.e., temperature of maximum pyrolytic hydrocarbon release from the kerogen, represented by a so-called S2 peak) were analyzed at the Research Institute of Petroleum Exploration & Development in Beijing using Rock–Eval pyrolysis.

3. RESULTS

3.1. Bulk geochemical characteristics

The TOC content of the black shales varies from 1.79% to 4.10%, while the stromatolitic carbonate and interbedded marl have significantly lower TOC values of 0.12% and 0.19%, respectively (Table 1). Rock–Eval pyrolysis revealed T_{max} values between 437 and 446 °C and hydrogen index (HI) values in the range of 150–352 (Table 1). These values place samples within the oil window and confirm their suitability for organic geochemical analyses. The black shales and interbedded marl have similar $\delta^{13}C_{org}$ and $\delta^{15}N_{org}$ values, varying around −33‰ (VPDB) and +2‰ (air), respectively (Table 1), while the concentrations of redox sensitive trace elements are also shown in Table 1.

3.2. Saturated hydrocarbons

Bitumen I of both exterior and interior sample portions, as well as the Bitumen II of interior sample portions are characterized by highly similar hydrocarbon distribution patterns and the following description focuses on the Bitumen I of interior portions unless otherwise specified. All samples yielded rich solvent extracts that, particularly for the black shales, were characterized by a dark color. Total ion chromatograms (TIC) of the saturated hydrocarbon fraction (Bitumen I, Interior) are shown in Fig. 2. All samples are characterized by distinct unresolved complex mixture (UCM) humps, whose positions vary among the different samples (Fig. 2). Except for the stromatolite sample, in which hopanes are visible in the TIC, all the other samples were dominated in the TIC by short-chain *n*-alkanes, monomethylalkanes and *n*-alkylcyclohexanes (Fig. 2). Steranes were not detected in any of the Bitumen I extracts, even when analyzed by GC–MS with MRM. Small traces of diasteranes were found in the Bitumen II of black shale interiors, while regular steranes were below the detection limit. Neither regular steranes nor diasteranes were detected in the Bitumen II of the stromatolitic carbonate or the marl (Fig. 5).

3.2.1. Alkanes, acyclic isoprenoids and n-alkylcyclohexanes

The *n*-alkane profile is dominated by low-molecular-weight compounds with maxima at C_{15} to C_{18} (Fig. 2), while mid-chain branched monomethylalkanes and *n*-alkylcyclohexanes are present with a similar distribution pattern. The ratio of *n*-alkylcyclohexanes to *n*-alkanes varies between 0.36 and 0.48 (Table 2; calculated on C_{20}). The stable carbon isotopic composition of the *n*-alkanes varies from −32.1‰ to −35.1‰ (Table 4). The concentration of acyclic isoprenoids such as pristane (Pr) and phytane (Ph) is exceedingly low in all analyzed samples (Fig. 2, Table 2). The $(Pr + Ph)/(C_{17} + C_{18})$ ratios of the Xiamaling black shale are ~0.1, which is significantly lower than the value of this parameter in the 1.1 Ga old Taoudeni black shales, or in some samples from the 1.64 Ga Barney Creek Formation (Summons et al., 1988b; Brocks et al., 2005; Blumenberg et al., 2012), but similar to other sediments in the Roper Basin (Summons et al., 1988b).

3.2.2. Hopanoids

Except for the stromatolite, none of the samples exhibited discernible peaks for hopanes when analyzed in full scan mode. In MRM mode, hopanes ranging from C_{27} to C_{35} were detected in all samples and were generally dominated by C_{30} 17α(H),21β(H)-hopane (Fig. 3). The 22S/(22R + 22S)-isomerisation ratios for C_{31} homohopanes were about 0.6 (Table 2) and the Ts/(Ts + Tm) (Ts: C_{27} 18α(H)-22,29,30-trisnorneohopane, Tm: C_{27} 17α(H)22,29,30-trisnorneohopane) ratios of the samples varied from 0.67 to 0.85 (Table 2). The homohopane index (HHI), i.e., the ratio of C_{35} to the sum of C_{31} to C_{35} 22S and 22R homohopanes, was in the range from 0% to 9.8% (Table 2). A significant negative correlation exists between the HHI and Ts/(Ts + Tm) (R^2 of 0.86; Fig. 4B).

Table 2
Selected hydrocarbon-based parameters of the samples analyzed in this study. See the text for the abbreviation for each parameter. The asterisk (*) indicates the ratio of C_{20} *n*-alkylcyclohexane to *n*-alkane.

Sample	Pr/Ph	Pr/*n*-C_{17}	Ph/*n*-C_{18}	$(Pr + Ph)/(n\text{-}C_{17} + n\text{-}C_{18})$	2-MHI	3-MHI	C_{20}*n*-alkyl/*n*-alkane*	HHI	C_{30}DiaH/(DiaH + H)	Ts/(Ts + Tm)	C_{31}H S/(S + R)	2MPI	C_{29} Ts/(H + Ts)
XML_strom.	0.18	0.04	0.13	0.09	1.1	5.2	0.35	7.5	0.30	0.67	0.59	0.30	0.46
XML_marl	1.04	0.16	0.20	0.18	0	0	0.46	0	0.33	0.85	0.64	0.51	0.42
XML_BS_4	1.27	0.16	0.10	0.13	5.7	5.8	0.39	4.6	0.68	0.77	0.53	0.46	0.69
XML_BS_3	0.24	0.04	0.24	0.17	2.6	5.7	0.43	9.8	0.69	0.68	0.57	0.42	0.57
XML_BS_2	0.88	0.09	0.14	0.11	8.1	4.7	0.48	8.1	0.55	0.71	0.54	0.41	0.51
XML_BS_1	1.07	0.07	0.10	0.08	4.6	2.2	0.38	5.3	0.56	0.72	0.57	0.54	0.57

Table 3
Comparison of some hydrocarbon ratios between the bitumen I of exterior, interior and bitumen II of interior.

Sample		Ts/(Ts + Tm)	C_{30} DiaH/(DiaH + H)	C_{31}H S/(S + R)	HHI (%)	C_{29} Ts/(H + Ts)
XML_strom.	Exterior	0.67	0.35	0.6	7.2	0.47
	Interior	0.67	0.30	0.59	7.5	0.46
	B II	0.66	0.30	0.6		0.42
XML_marl	Bulk	0.85	0.33	0.64	0	0.42
	BII	0	0	0	0	0
XML_BS_4	Exterior	0.76	0.61	0.57	4.9	0.62
	Interior	0.77	0.68	0.53	4.6	0.69
	B II	0.75	0.62	0.56	6.7	0.59
XML_BS_3	Exterior	0.68	0.67	0.56	12.4	0.51
	Interior	0.69	0.69	0.57	9.8	0.57
	B II	0.76	0.67	0.57	6.2	0.59
XML_BS_2	Exterior	0.71	0.65	0.52	11.6	0.62
	Interior	0.71	0.55	0.54	8.1	0.51
	B II	0.72	0.69	0.61	8.2	0.49

Table 4
Compound-specific carbon isotopic composition of *n*-alkanes extracted from four of the samples used in this study. The bulk organic carbon isotopic composition was according to Luo et al. (2014). A dash (–) indicates that the concentration was too low to yield reliable results.

Sample	XML_BS_1		XML_BS_3		XML_BS_4		XML_marl	
	$\delta^{13}C$	±(1σ)	$\delta^{13}C$	±(1σ)	$\delta^{13}C$	±(1σ)	$\delta^{13}C$	±(1σ)
n-C_{13}	–	–	–	–	−34.2	0.1	−33.2	0.1
n-C_{14}	–	–	–	–	−35.1	0.3	−32.1	0.0
n-C_{15}	–	–	–	–	−34.5	0.2	−32.5	0.2
n-C_{16}	−32.4	0.1	–	–	−34.4	0.4	−32.7	0.2
n-C_{17}	−33.1	0.1	−33.4	1.0	−33.8	0.0	−32.7	0.1
n-C_{18}	−33.1	0.1	−34.5	0.6	−34.0	0.3	−33.1	0.1
n-C_{19}	−32.6	0.3	−32.8	0.5	−33.7	0.4	−33.0	0.1
n-C_{20}	−32.6	0.2	−32.8	0.8	−33.8	0.5	−33.4	0.0
n-C_{21}	−32.2	0.2	−34.7	1.0	−34.0	0.7	−33.1	0.2
n-C_{22}	−32.3	0.4	–	–	−34.2	1.3	−32.7	0.4
n-C_{23}	−31.6	0.3	–	–	−32.3	0.9	−32.8	0.1
n-C_{24}	−31.6	1.3	–	–	−34.0	0.8	−32.7	0.2
Bulk	−32.8	0.1	−33.6	0.1	−34.1	0.1	−33.1	0.1

Except for the common rearranged hopanes Ts and C_{29} Ts, we observed two other series of rearranged hopanes in all samples, which follow a similar chromatographic pattern to the αβ-hopanes but which elute earlier (Fig. 3). Comparison of retention times and elution sequence to published data (Moldowan et al., 1991; Farrimond et al., 1998; Zhu et al., 2007), allowed us to identify the series eluting directly before the αβ-hopanes (peaks B1 to B8 in Fig. 3) as 17α(H)-diahopanes (including the C_{27} and C_{29}–C_{35} members). The identity of the other series (peaks C1 to C7 in Fig. 3), which elute much earlier and which are generally lower in concentration than the 17α(H)-diahopanes, is unclear at present. They are termed rearranged-X here, for convenience. The ratio of C_{30} 17α(H)-diahopane to C_{30} αβ-hopane (C_{30} Dia/(Dia + H)) is about 0.6 in black shales and therefore much higher than that in the carbonate and marl samples, which are characterized by values less than 0.33 (Table 2). A positive correlation ($R^2 = 0.75$, $n = 6$) is observed between the C_{30} Dia/(Dia + H) and C_{29} Ts/(Ts + H), while no relationship exists between the C_{30} Dia/(Dia + H) and Ts/(Ts + Tm) (Fig. 4A, D).

Both 2α-methylhopanes and 3β-methylhopanes were detected in the analyzed samples (Table 2), with 2α-methylhopane indices (2-MHI, i.e., the ratio between C_{31} 2α-methylhopane and the sum of C_{31} 2α-methylhopane and C_{30} αβ-hopane) ranging from 2.2% to 8.1% in the black shales, but being significantly lower in the carbonate (1.1%) and marl (0%). The 3β-methylhopane index (3-MHI, i.e., the ratio between C_{31} 3β-methylhopane and the sum of C_{31} 3β-methylhopane and C_{30} αβ-hopane) values vary from 0% to 5.8% without any distinct lithological correlation (Table 2).

3.2.3. Tricyclic terpanes

Tricyclic terpanes ranging from C_{19} to C_{26} were detected in all samples (Fig. 6A), while an additional series of tricyclic terpanes, characterized by *m/z* 123 and dominated by C_{19} (Fig. 6B), was found in the stromatolitic carbonate. Comparison of the mass spectra and relative retention times of this series of terpanes with previously published data (Wang and Simoneit, 1995) leads us to identify them as 13α(alkyl)-tricyclic terpanes. In the black shale, the concentration of this series of tricyclic terpanes is exceedingly low,

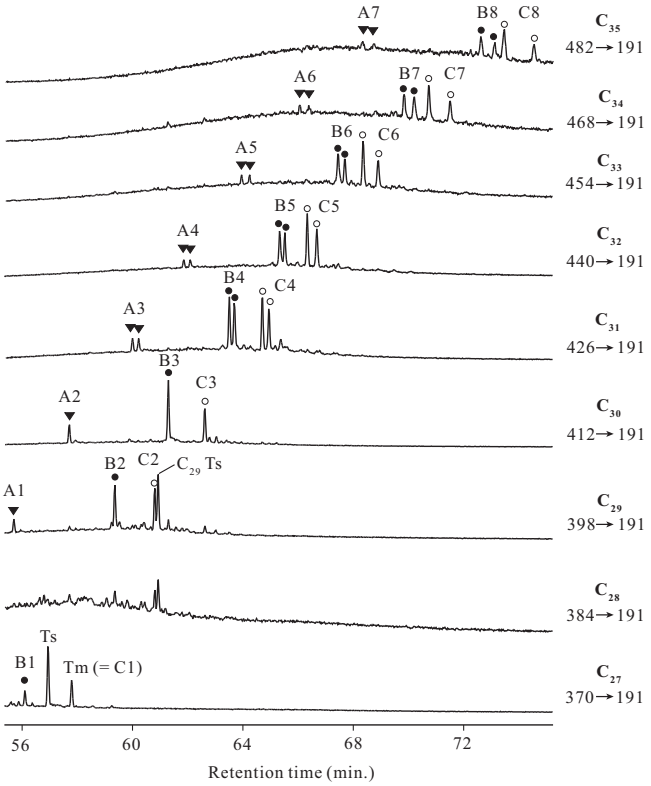

Fig. 3. The distribution pattern of hopanes in one of the black shales (XML_BS_3) as analyzed by MRM. Blank circles: 17α(H),21β(H)-hopanes; Solid circles:17α(H)-diahopanes; Solid triangles: rearranged hopanes. Ts: C_{27} 18α(H)-22,29,30-trisnorneohopane, Tm: C_{27} 17α(H)22,29,30-trisnorneohopane.

although the predominance of the C_{19} isomer appears to persist.

3.3. Aromatic hydrocarbons

In all samples, the most abundant aromatic compounds are 3–4 ring polycyclic aromatic hydrocarbons (PAHs) and their methylated counterparts, including phenanthrene (P), fluoranthene (Fla), pyrene (Pyr) and chrysene (Chy). Fluorene (F), dibenzofuran (DBF) and dibenzothiophene (DBT) were detected only in the stromatolite sample, while absent in any of the black shales. No aromatic steroids or aromatic carotenoids, specifically isorenieratane and its derivatives, were detected in any of the samples.

4. DISCUSSION

4.1. Syngenicity of biomarkers

A syngenetic relationship of the bitumen to its host rock is a prerequisite for any discussion on the reconstruction of paleo-sedimentary environments and paleoecology on the basis of hydrocarbon biomarkers. Especially in light of the growing awareness of contamination risk for organic lean samples (e.g., Brocks, 2011; Illing et al., 2014) it is important to warrant the reliability of data. Apart from the fact that all samples yielded high abundances of a dark colored extract and carry molecular characteristics that are typical for Proterozoic bitumens (Summons et al., 1988b; Summons and Walter, 1990; Dutkiewicz et al., 2003, 2006; Brocks et al., 2005; Blumenberg et al., 2012; Pawlowska et al., 2013), i.e., a large UCM and high relative abundance of branched alkanes, we performed targeted experiments to assess the syngenicity of components reported herein. In particular, comparing sample interiors *vs.* exteriors, on one hand, and Bitumen I *vs.* Bitumen II, on the other, revealed that all extracts are virtually identical in terms of composition and concentration, and concentrations well above any of the procedural blanks (Fig. 7, Table 3). The non-detection of regular steranes strengthens the notion that no contamination with Phanerozoic organic matter has occurred and a high similarity in stable carbon isotopic composition of the *n*-alkanes to that of the co-occurring kerogens (within 2‰; Table 4) suggest a genetic relationship. Furthermore, the thermal maturity of the bitumen, as reconstructed from molecular parameters, falls in the same range as that of the kerogen, indicated by T_{max} values (see below), while significant and systematic molecular differences between deep-water black shales and carbonates deposited in shallower environments exclude a migrated origin of the bitumens.

It should be noted that traces of diasteranes were found in the bitumen II of the black shales, while the corresponding regular steranes were below detection limit (Fig. 5). The fact that steroidal molecules were not found in procedural blanks, any of the other samples or in the Bitumen I of the black shales indicates an indigenous origin and it is possible to speculate about preferential preservation of certain

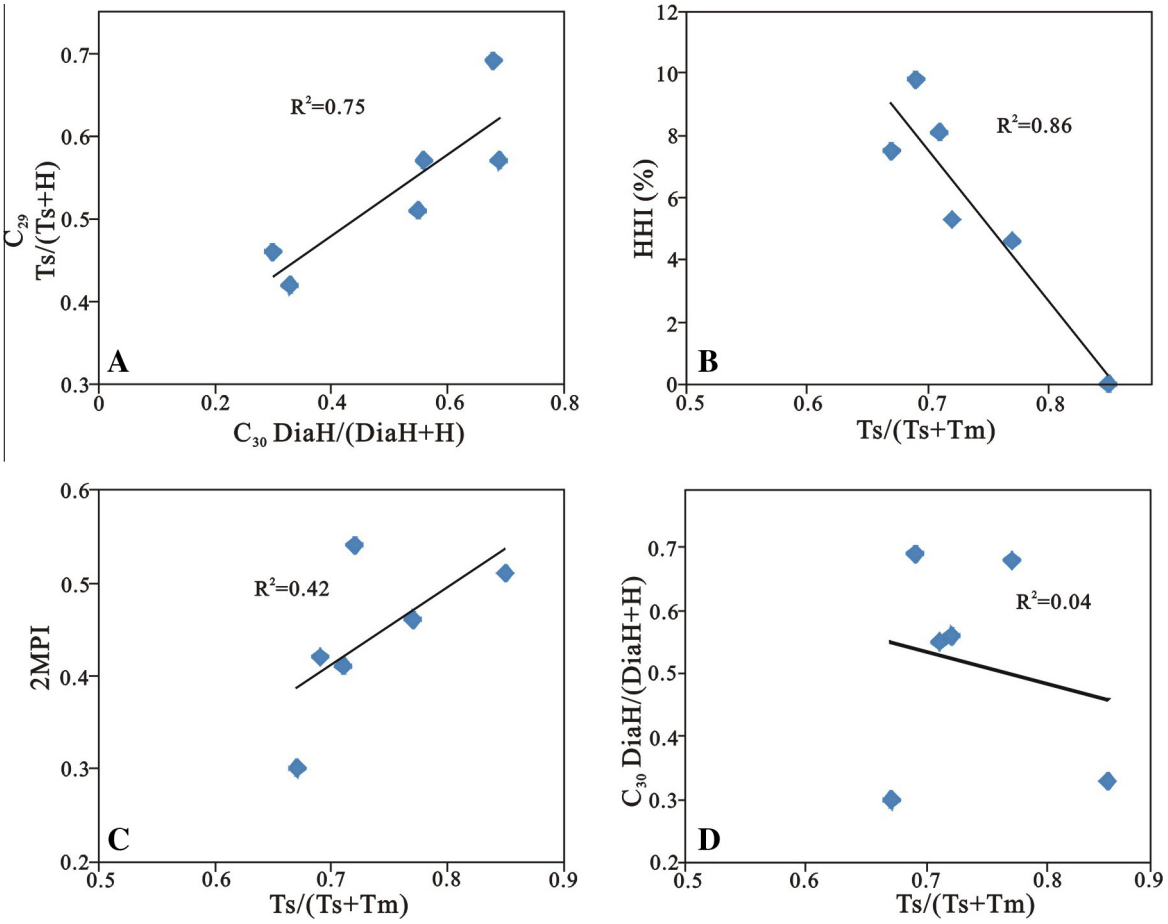

Fig. 4. Cross-plots of hopanoid ratios (A, B, D) and hopanoid ratios and the methylphenanthrene index (2-MPI) (C). DiaH: 17a(H)-diahopane;

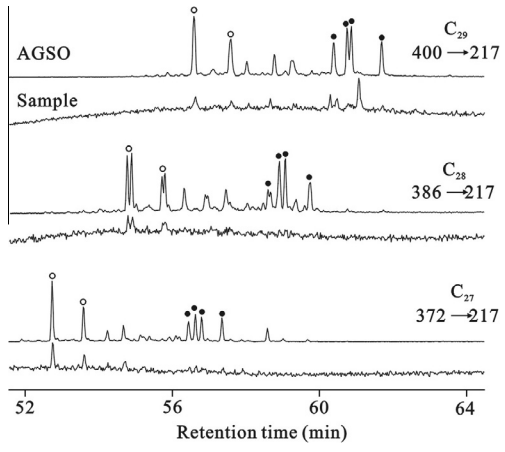

Fig. 5. Pairs of GC–MS (MRM) chromatograms for the analysis of steranes in bitumen II of one black shale (XML_BS_4). All chromatograms are shown to the same absolute scaling. The top trace represents the AGSO oil standard for referencing with the equivalent data for the sample in the lower trace. Blank circle: diasteranes; Solid circle: regular steranes.

molecules in Bitumen II, which is attributable to the known enhanced preservation in association with clay minerals, as has been well established for sedimentary rocks throughout the geological record (e.g., Rubinstein et al., 1975; Sieskind et al., 1979; van Kaam-Peters et al., 1998; Peters et al., 2005).

4.2. Oil-window thermal maturity and alternate controls on norneohopane abundances

All samples yielded internally consistent molecular data regarding the degree of their thermal overprint. Isomerization at position C-22 in the homohopane side-chain reaches a stable value around 58–60% of the 22S/(22S + 22R) ratio before the main phase of petroleum generation (Peters et al., 2005) and amounts to values between 53% and 59% in the studied samples (Table 2), placing the Xiamaling Fm. in the upper oil window. Another common maturity proxy, the methylphenanthrene index (MPI), which compares the decrease of less stable methyl-aromatic isomers due to steric hindrance (Radke and Welte, 1981; Boreham et al., 1988), ranges from 0.41 to 0.54 (Table 2). According to the regression equation calibrated by Boreham et al. (1988), the calculated vitrinite reflectance equivalent (Rc) is about 0.6% and thus also places the analyzed samples in the oil window. This relatively low thermal maturity, relative to the geological age of samples, is in agreement with

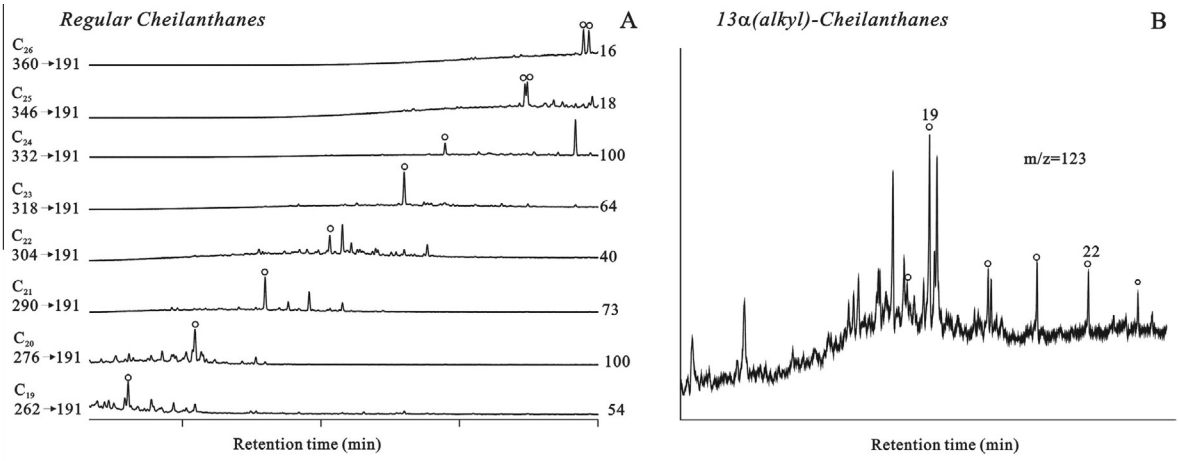

Fig. 6. (A) GC–MS (MRM) chromatograms showing regular tricyclic terpanes present in both the black shale and carbonate stromatolite. The number on the right side of each chromatogram is the scaling factor based on relative response of the tallest peak in the regular cheilanthanes. (B) The novel tricyclic terpanes (13α(alkyl)) that present only in the stromatolite are shown by $m/z = 123$, as analyzed by conventional GC–MS. The numbers above the peaks represent the carbon number of each compound.

the absence of detectable adamantane and diamantane molecules, which are typically present in highly mature bitumens (Chen et al., 1996) and consistent with T_{max} and HI values obtained on kerogens by Rock Eval pyrolysis (Table 1).

While the Ts/(Ts + Tm) ratio is frequently used as a thermal maturity index, it can be affected by other factors such as host rock lithology and depositional environmental conditions (Moldowan et al., 1986; Peters et al., 2005). The samples in this study have relatively high and consistent Ts/(Ts + Tm) ratios, generally above 65%, that lack any distinct stratigraphic or lithological trend (Table 2) and do not appear to be primarily affected by thermal maturity, as indicated by the absence of any relationship with the MPI (Fig. 4C) or the C_{31} homohopane 22 S/(S + R) molecular parameters. It has been suggested that the Ts/(Ts + Tm) ratio is only a reliable indicator of thermal maturity when comparing samples of the same litho- and organofacies (Peters et al., 2005) since clay mineral-catalyzed diagenetic reactions may control the formation of neohopanes, leading to low values in carbonate source rocks (McKirdy et al., 1981; Rullkötter et al., 1985). Yet hypersaline (Rullkötter and Marzi, 1988) and low-Eh environments (Moldowan et al., 1986) tend to be characterized by exceedingly high values in the ratio. As mentioned in Section 3.2.2 and shown in Fig. 4B, samples from the Xiamaling Fm exhibit a negative linear correlation between the Ts/(Ts + Tm) ratio and the homohopane index (HHI), suggesting that in this depositional environment the Ts/(Ts + Tm) values are influenced primarily by either biological input or, more likely, environmental Eh. Given the limited sample set and a relatively narrow range of values for both parameters, the occurrence of a similar linear relationship should be monitored in future studies to shed more light on possible controls of this commonly used thermal maturity parameter.

4.3. Origin of the diahopanes

All of the samples analyzed here contain uncommonly high concentrations of rearranged 15α-methyl-27-norhopanes (aka. *hopanes or 17α(H)-diahopanes; Fig. 3, Table 2). Additionally, most of the samples contain a third, uncommon series of putatively rearranged hopanes—albeit in much lower concentration—characterized by a similar chromatographic distribution pattern to that of hopanes and diahopanes (Fig. 3). Diahopanes have been reported in a large variety of sedimentary rock types from different time periods (Pratt et al., 1991; Telnaes et al., 1992; Farrimond et al., 1998; Zhu et al., 2007; Dutta et al., 2013), including in high abundances in Precambrian sediments (e.g., Summons et al., 1988a,b; Blumenberg et al., 2012). Yet to date, the origin of diahopanes remains unresolved (Dutkiewicz et al., 2003; Smith and Bend, 2004; Zhu et al., 2007). Initial attribution to terrigenous sources (e.g., Philp and Gilbert, 1986; Telnaes et al., 1992) gave way to the finding that diahopanes likely form by catalytic rearrangement of regular bacterial hopanoids on acidic sites of clay minerals during diagenesis (Moldowan et al., 1991).

The C_{30} Dia/(Dia + H) values of the samples in this study vary from 0.30 to 0.69 (Table 2). These values are much higher than those found in black shales of the 1.1 Ga Atar Group, which have a similar thermal maturity (Blumenberg et al., 2012) or those found in 1.4 Ga oil inclusions within the Roper Group (Dutkiewicz et al., 2003). Neither thermal maturation nor microbial degradation can explain the enhanced formation of diahopanes in the Xiamaling Formation. The fact that we find higher values of C_{30} Dia/(Dia + H) in the black shales than in the carbonate and marl supports the hypothesis that the formation of diahopanes is related to catalysis on clay minerals (Moldowan et al., 1991), yet it remains unclear why the C_{30} Dia/(Dia + H) values show a distinct positive relationship with C_{29} Ts/(Ts + H), but not with Ts/(Ts + Tm)

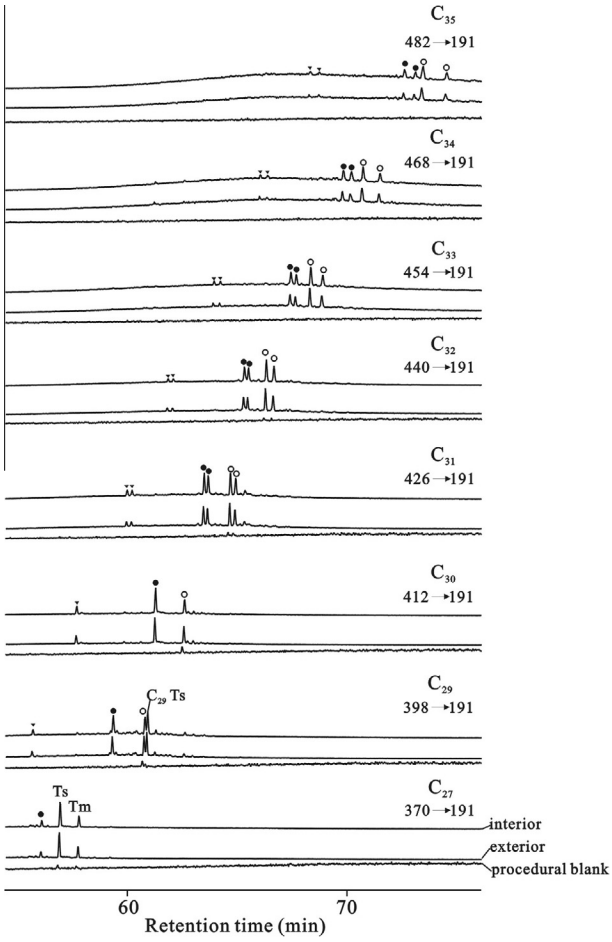

Fig. 7. Comparison of hopanes between the procedural blank, bitumen I of exterior and interior of a black shale sample (XML_BS-3), as determined by GC–MS (MRM) analysis. All chromatograms are shown to the same absolute scaling. Blank circle: 17α(H),21β(H)-hopane; Solid circle: 17α(H)-diahopanes; Solid triangles: rearranged hopanes with unknown structure.

(Fig. 4A, D). We cannot exclude the possibility that the enhanced abundance of diahopanes could be attributable to the existence of a specific biological precursor. By analogy to the fact that diasteranes are derived from diasterenes, in turn originating from steroidal alkenes during early diagenesis (e.g., Peakman and Maxwell, 1988), it is possible that diahopanes are formed from unsaturated precursors such as the Δ-6 or Δ-11 unsaturated bacteriohopanes that have only been observed in a limited number of bacterial taxa (e.g., Rohmer and Ourisson, 1986; Talbot et al., 2007).

4.4. Anoxic depositional environments of the Xiamaling Formation

It has long been speculated that Mesoproterozoic marine basins witnessed a higher frequency of anoxic and strongly stratified conditions, where bottom waters were either sulfidic (Canfield, 1998; Shen et al., 2003; Brocks et al., 2005) or ferruginous (Poulton et al., 2010; Planavsky et al., 2011; Luo et al., 2014). Cross-plots showing the trace elemental ratios of V/(V + Ni), V/Cr and Th/U in studied samples (Fig. 9) indicate that all of the black shales from the Xiamaling Formation were deposited in anoxic environments (Hatch and Leventhal, 1992; Jones and Manning, 1994), with two samples bordering the euxinic field. High Mo concentrations (>10 ppm *vs.* 1 ppm of the crustal average value) support the deposition in anoxic environments. But Mo values are still significantly lower than those recorded in older sediments that were deposited under euxinic conditions—black shales in the 1.84 Ga Rove Formation, for example, are characterized by values up to 62 ppm (Scott et al., 2008). The absence of aryl isoprenoids, biomarkers from green and purple sulfur bacteria, and organosulfur compounds such as dibenzothiophene, which are principally formed by incorporation of reduced sulfur and sulfur radicals during early diagenesis (Hughes et al., 1995; Werne et al., 2008), argues against the prevalence of euxinic conditions and in favor of low environmental sulfate concentrations. This is reconcilable with the generally accepted scenario of a small global marine sulfate pool at this time in Earth history (Kah and Bartley, 2011). Anoxic depositional conditions are supported by low values (generally <1.0) in the pristane over phytane ratio (Pr/Ph; Didyk et al., 1978) and relatively high values for the HHI (4.6–9.8%) (Köster et al., 1997). Both the Pr/Ph and HHI, which are 0.18 and 7.5%, respectively, suggest that also the stromatolite formed in an anoxic environment. The HHI values presented here are a little lower than those in typical euxinic environments, such as the Monterey oil (Peters and Moldowan, 1991) and P–Tr transition (Cao et al., 2009). This could be ascribed to the non-euxinic environment during the deposition of the Xiamaling Fm. Under conditions of very low sulfate, concentration, for example, as in Phanerozoic freshwater lacustrine environments, this enhanced preservation of higher hopane homologs does not occur, probably because the appropriate mechanism for sulfur incorporation was not operative (Peters and Moldowan, 1991).

The likely absence or ecological insignificance of phototrophic sulfur bacteria during deposition of the Xiamaling Fm has another consequence for interpretations. Remnants of their carotenoids, i.e., aryl isoprenoids, in sediments typically indicate euxinia in the photic zone (Summons and Powell, 1987)—which is often interpreted to specify the upper water column. Yet green sulfur bacteria contain a fairly unique light-harvesting machinery that allows them to persist at low photon fluxes (e.g., Beatty et al., 2005) and as a consequence many depositional environments, probably including those represented in the Xiamaling Fm, were shallow enough to receive sufficient solar radiation at the sediment–water interface to allow the existence of phototrophic sulfur bacteria. In fact, most microbial mats contain green sulfur bacteria (e.g., Nicholson et al., 1987; Overmann, 2006) and recently it was found that even purple sulfur bacteria, previously considered to consist of only planktonic species (Brocks and Schaeffer, 2008), are likely represented in benthic microbial mats (French et al., 2013). In addition, the almost-ubiquitous presence of aryl isoprenoids in sediments of all ages likely highlights

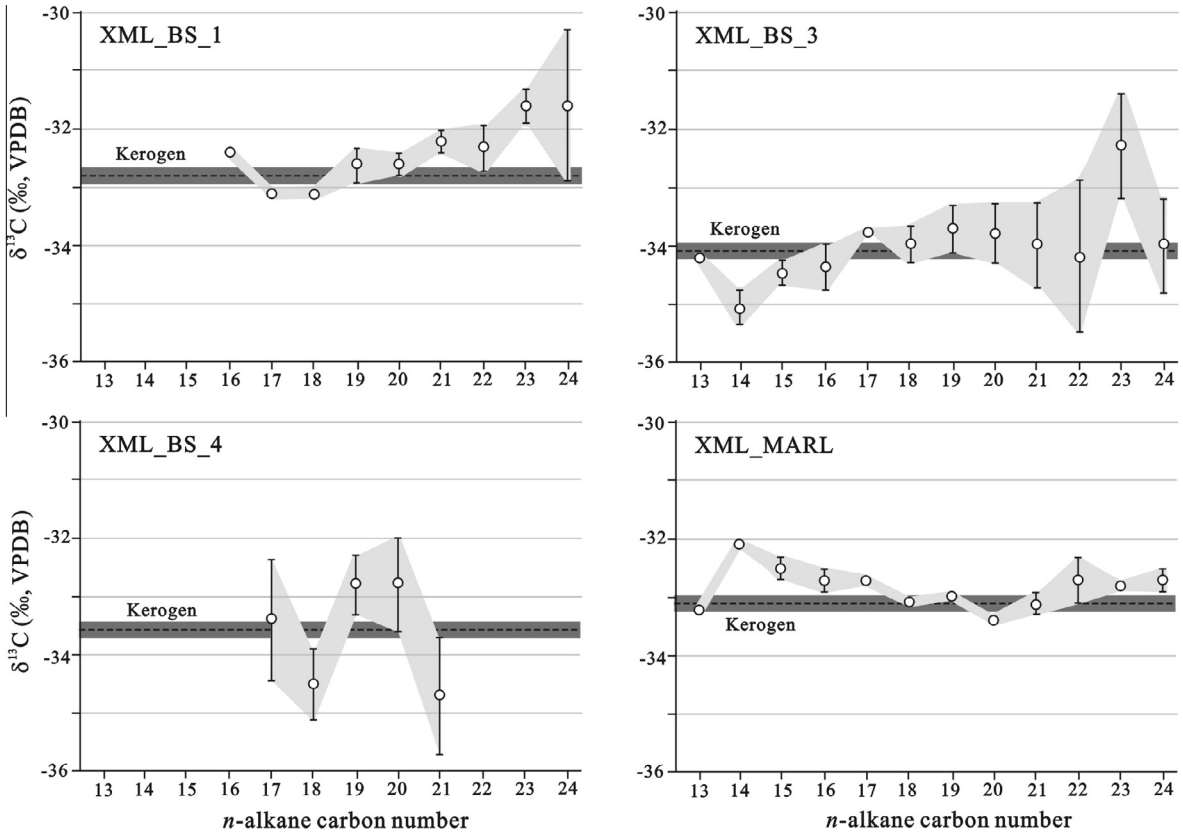

Fig. 8. Relationship between the $\delta^{13}C$ of *n*-alkanes and kerogen in the Xiamaling black shale samples. The bulk organic carbon isotopic composition was reported previously by Luo et al. (2014).

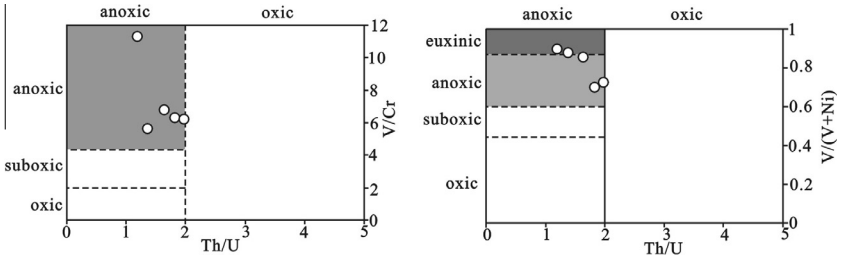

Fig. 9. Cross-plots between redox-related trace element ratios according to Hatch and Leventhal (1992). The low values (<2.0) of the Th/U ratio and high values (>4.5) of the V/Cr ratio suggest all the samples were formed in anoxic environments. The V/(V + Ni) values indicate that most of the samples were deposited in anoxic but not sulfidic environments.

the importance of benthic microbial mats (French et al., 2013). This finding renders it all the more significant that the Xiamaling Fm. lacks either visual evidence of microbial mat formation in the studied samples or any measurable aryl isoprenoids, which—if present—should have been well preserved from a taphonomic perspective.

4.5. Microbial degradation and the origin of the large unresolved complex mixture (UCM)

The chromatographic profiles of all samples in this study exhibit a significant 'hump' of UCM. Together with low relative abundances of phytanyl lipids, such humps (Fig. 2) are typical of Proterozoic bitumens and attributed to microbial re-working and biodegradation of the organic matter. This scenario is expected to be much more distinct in the stromatolitic carbonate when invoking the 'mat-seal effect' proposed by Pawlowska et al. (2013), which could be one of the factors responsible for the low concentration of Pr and Ph and the absence of steroids in the Xiamaling stromatolite (Fig. 2). A putative mat-seal effect would be rather unlikely to affect the lipid composition in the black shales, which were deposited in much deeper water environments (Wang and Li, 1993), although microbial re-working in the water column could have been extensive as hypothesized by Logan et al. (1995).

During the subsurface anaerobic biodegradation of bitumen or petroleum fluids, normal alkanes typically

disappear first, followed by (with certain overlap) acyclic and then cyclic isoprenoids (Volkman, 1983; Peters et al., 2005). The presence of *n*-alkanes in all of the studied samples is contradicted by the significant UCM, since during the stage in which the UCM becomes prominently visible in chromatograms, all *n*-alkanes have typically been depleted (Hallmann et al., 2008). Currently existing models which might explain the prevalence of such bitumens involve strong heterotrophic reworking of primary produced biomass, either within the water column (Logan et al., 1995) or after settling on (partially oxygenic) benthic microbial mats (Pawlowska et al., 2013). In both scenarios phytanyl lipids and well as steroids that are produced in surface waters are degraded during multiple heterotrophic cycles, yet not replenished by these subsequent communities. Alkyl lipids, on the contrary are degraded but reintroduced to the sinking organic matter pool by fresh heterotrophic biomass that is increasingly enriched in ^{13}C relative to the catabolized substrate (DeNiro and Epstein, 1978). It is generally assumed that the bulk of the sedimentary kerogen represents polymerized biomass from photosynthetic primary producers (Logan et al., 1995; Close et al., 2011) since heterotroph biomass production can only constitute a small proportion of total productivity. In this scenario, the stable carbon isotopic composition of alkyl lipids would be expected to be heavier than that of either phytanyl lipids or bulk kerogen, which is considered a typical characteristic for many Precambrian bitumens (Logan et al., 1995). Williford et al. (2011), for example, showed that sediments from the 1.64 Ga Barney Creek Fm., whose lipid inventory is widely accepted to be uncontaminated, do exhibit a 5–6‰ anomalous isotopic offset between kerogen and *n*-alkanes.

In the Xiamaling black shale, however, most *n*-alkane $\delta^{13}C$ values closely match those of the co-existing kerogen within the range of calculated error (Fig. 8, Table 3). One possibility for the co-occurrence of strong signs of biodegradation with a carbon isotopic similarity between kerogen and individual lipids could be that the majority of preserved biomass—both lipids and kerogen—derives from benthic heterotrophs, thus indicating complete reworking of pelagic and benthic organic matter. Such high trophic recycling would only be possible if the proportion of recalcitrant organic matter in pelagic biomass would have been very low which is rather improbable, although it requires further investigation. On the other hand, it is exceedingly hard to envisage how up to ~4% of TOC could be created solely from heterotrophic biomass. Close et al. (2011) modeled that a shift from prokaryote-dominated community to a heterogeneous community of pro- and eukaryotic primary producers could also lead to the disappearance of the characteristic inverse isotope signal. As discussed above, the abundance of eukaryotes indicated by steranes was very low in the Xiamaling Formation. Furthermore, samples from the Mesoproterozoic Taoudeni Basin (1.1 Ga; Blumenberg et al., 2012) for example exhibit both, pronounced positive and negative carbon isotopic ordering with respect to kerogen and lipids, apparently decoupled of depositional redox and other molecular parameters and all in the presence of a persistent UCM.

Due to these discrepancies we prefer to interpret the large UCM as not being the direct result of biodegradation but rather, indicative of significantly enhanced isomerization of all the organic molecules present over the long burial history of these rocks. In exploring alternative explanations we refer to the very fundamental question of kerogen formation, which has still not been settled and, in large part, oscillates between the preservation of large and degradation-resistant biopolymers (e.g., de Leeuw and Largeau, 1993) and the repolymerization of smaller compounds (e.g., Huc, 1980), likely aided by vulcanization-like reactions involving sulfur (e.g., Sinninghe-Damsté et al., 1998; van Kaam-Peters et al., 1998). Although speculative, it is becoming increasingly clear that alternative explanations for typical Proterozoic bitumen fingerprints are needed and, with this previous suggestion, we encourage continued exploration of unconventional possibilities.

In addition to microbial degradation, an alternative explanation is required for exceptionally low relative phytanyl lipid abundances. In geological samples Pr and Ph are mainly derived from the phytol side chain of chlorophyll produced by phototrophic microbes, with an additional but frequently negligible contribution from archaeal isoprenoids and tocopherols (Goossens et al., 1984; ten Haven et al., 1987). We propose that the low $(Pr + Ph)/(C_{17} + C_{18})$ values might be the result of the presence of anoxygenic phototrophic bacteria that used alternative esterifying alcohols in their chlorophylls. For example, the light-harvesting antennae of green bacteria employ a variety of ester groups, including those with long straight chains, in their bacteriochlorophylls (Tamiaki et al., 2007). Other types of autotrophic organisms, such as chemolithoautotrophic microbes may have contributed to the organic matter content in the black shales (Luo et al., 2014) and our picture of the relevance and/or preservation of phototrophs might be skewed by using only the phytanyl lipids Pr and Ph as molecular proxies.

4.6. Microbial facies of the Xiamaling Formation

The absence of detectable steranes in the Bitumen I of the Xiamaling Fm. is consistent with several recent studies that failed to detect steranes in Precambrian black shales between ~1.1 and ~1.6 Ga (Dutkiewicz et al., 2003; Brocks et al., 2005; Blumenberg et al., 2012), which suggests that eukaryotes were very low in abundance and could not have been the main biotic precursors of the high OC content in the black shale. This could be due to the fact that eukaryotes had not yet risen to ecological significance (e.g., Knoll et al., 2006) or because they occupied littoral environmental niches not favorable to the preservation of organic matter (Javaux et al., 2001, 2004). Yet Bian et al. (2005) reported a high abundance of microfossils from the Xiamaling black shale, which they attributed to benthic red algae and proposed as the main biotic source of organic matter in this unit. If correct, it would indicate that some types of eukaryotic algae were abundant in this time interval, which seems inconsistent with the absence or very low concentration (below detection limit) of steranes in the

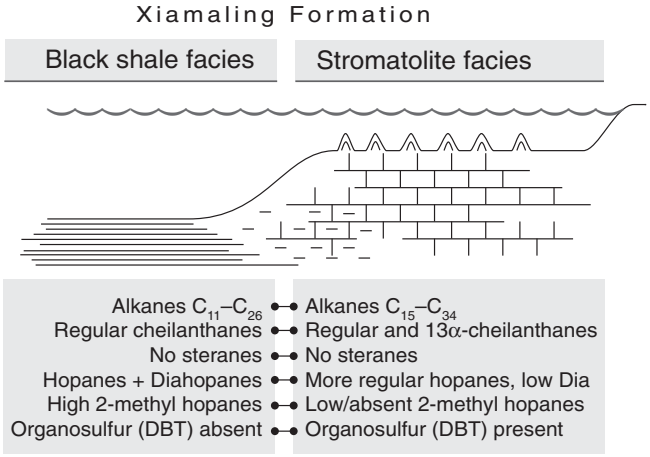

Fig. 10. Comparision of the hydrocarbon composition between the stromatolite and black shale in the Xiamaling Formation.

black shale as found in our study. This observation is supported by hydropyrolysis experiments, which revealed that bitumens that are artificially released from the kerogen network by catalytic cracking also do not contain any steranes (Dr. Gordon Love, personal communication). While more work needs to be undertaken in order to test the biological affiliation of the microfossils found in the Xiamaling Formation, the apparent discrepancy between molecular and microfossil eukaryotic records is an interesting question and possibly the result of taphonomic bias.

Although C_{30} and lower carbon-numbered hopanes may be derived from diploptene or diplopterol, which are synthesized by diverse organisms including bacteria (Ourisson et al., 1987; Summons et al., 1994), homohopanes are known to derive exclusively from the C_{35+} bacteriohopanepolyols formed by various clades of bacteria (Rohmer et al., 1984; Pearson et al., 2007; Welander et al., 2012; Ricci et al., 2014). The high relatively concentration of hopanes suggests that bacteria would have been the predominant marine biota where these rocks were deposited. This is particularly evident in the case of the stromatolitic facies, in which hopane concentrations are significant, even in comparisons to linear alkanes, which form the principal hydrocarbons (Fig. 2). Although the exact function of hopanoids in bacteria is still not adequately understood (Doughty et al., 2009; Welander et al., 2010), a recent survey demonstrated a high overlap of bacteria synthesizing hopanoids and those being capable of nitrogen fixation (Pearson et al., 2007). Given that the stable nitrogen isotopic composition ($\delta^{15}N$) of the black shales in the Xiamaling Formation varies around 2‰ (Table 1), which is much lower than the $\delta^{15}N$ (~5‰) value of modern oceanic nitrate (Sigman et al., 2009) and falls within the range of nitrogen isotopic fractionation by diazotrophic cyanobacteria (e.g., Bauersachs et al., 2009), it allows the speculation that these microbes played a significant role in the water column from which the Xiamaling sediments settled—a hypothesis tentatively supported by relatively high concentrations of monomethylalkanes in the studied samples (Shiea et al., 1990; Talbot et al., 2008).

2α-methylhopanes originating from 2-methylbacteriohopanpolyols have been proposed as biomarkers for cyanobacteria (Summons et al., 1999). The 2-MHI values of the Xiamaling black shales vary from 2.6% to ~8.0% (Table 2), which is much higher than that of the carbonate stromatolite (1.1%). These values are similar to those of late Mesoproterozoic black shales in the 1.1 Ga Taoudeni Basin (Blumenberg et al., 2012), but much lower than those in black shales deposited during Cretaceous Oceanic Anoxic Events (OAEs) or after the Paleozoic mass extinctions, which are characterized by 2-MHI values as high as 30% (Kuypers et al., 2004; Xie et al., 2005; Cao et al., 2009). New knowledge about the biosynthesis of methylated hopanoids shows that both cyanobacteria and alphaproteobacteria can be sources of 2-methybacteriohopanpolyols (Welander et al., 2012). Another important factor to bear in mind when considering these data is that prominent nitrogen fixing cyanobacteria in today's oceans such as *Trichodesmium* and *Crocosphaera* sp. do not produce 2-methylbacteriohopanepolyols (Sáenz et al., 2012). Further, environmental surveys of both biosynthetic capabilities and hopanoid abundances indicate that organisms capable of producing 2-methylbacteriohopanepolyols are not prevalent in open ocean waters compared to coastal, lagoonal and terrestrial settings (Allen et al., 2010; Sáenz et al., 2011; Luo et al., 2013; Ricci et al., 2014). Genomic analyses of cultures and environmental samples offers a much improved approach to documenting the biotic precursors and distribution of 2-methylbacteriohopanepolyols.

The presence of 3β-methylhopanes suggests that type I aerobic methanotrophic bacteria or aerobic acetic acid bacteria were present in this system (Rohmer et al., 1984; Zundel and Rohmer, 1985). However, a recent survey of the C-3 methylase, the enzyme required for methylation at C-3 position of bacteriohopanepolyols, indicated a more diverse taxonomic distribution of 3β-methylbacteriohopanepolyols (Welander and Summons, 2012). Without compound-specific carbon isotopic composition data, which is currently impossible to obtain due to the low concentration of these compounds, the biotic precursors of the 3β-methylhopanes present in the Xiamaling Formation remain unclear. But it is likely that they originated from aerobic microbes (Welander and Summons, 2012). The 3-MHI of the Xiamaling black shale and stromatolite is

~5.2%, which is slightly higher than the Phanerozoic average values (~3%) (Rohrssen et al., 2013), and similar to those found in the latest Paleoproterozoic rocks in the McArthur basin (Brocks et al., 2005). This could be ascribed to low marine sulfate concentrations, which could have allowed higher rates of methanogenesis and, therefore, methanotrophy (Brocks et al., 2005; Luo et al., 2010).

While a number of molecular parameters differed between shallower carbonate dominated facies and basinal shales due to lithologically-induced rearrangements, it is interesting to observe that further systematic variability clearly points to differences in the microbial communities responsible for organic matter production (Fig. 10). Firstly, the relative concentration of hopanes is higher in the stromatolite—the full scan analyses of these extracts reveals hopanes even in the TIC, which is not the case for extracts of the black shales. Secondly, the 2-MHI value of the black shale is higher than that of the stromatolite. Thirdly, the C_{30} Dia/(Dia + H) value of the black shale is higher than that of the stromatolite although the origin of diahopanes is not presently understood. Fourth, the compositions of tricyclic terpanes are different. Except for the regular tricyclic terpanes, which were detected in both the black shale and stromatolite, a novel tricyclic terpane series (13α [alkyl] tricyclic terpanes) is present in the stromatolite but absent in the black shale (Fig. 6B). Wang and Simoneit (1995) found the same series of compounds in a bituminous sandstone that is located at the base of the Xiamaling Formation. Unfortunately, the biotic sources of this tricyclic terpane series remain unresolved and further investigation is warranted in order to further illuminate the sources of difference in microbial community composition between the stromatolite and black facies and their implications for paleoenvironmental reconstruction.

5. CONCLUSIONS

Abundant hydrocarbons of oil window thermal maturity were detected in black shales and a stromatolitic carbonate from the Xiamaling Formation in North China, and deemed to be syngenetic based on hydrocarbon compositions and concentration gradients. Low-molecular-weight *n*-alkanes peaking at C_{15} to C_{18}, relatively high concentration of hopanes and the very low contents of steranes suggest that bacteria were the main biotic precursors to the organic matter, yet subtle but distinct molecular differences are noted between the black shale and stromatolite facies, including relative concentration of hopanes, the presence of an uncommon series of tricyclic terpanes and a series of rearranged hopanes. This variation can be attributed to both, diagenetic rearrangement and to a differential microbial input. A persistently anoxic, yet non-sulfidic depositional environment was reconstructed from biomarker ratios and redox-sensitive trace elements. The observation of typical Proterozoic molecular characteristics, such as a large UCM, steranes only at trace levels and low abundances of phytanyl lipids in combination with the absence of a stable carbon isotopic offset between kerogen and alkanes warrants the proposal that existing explanatory models, involving extensive heterotrophy or a taphonomic bias associated to benthic microbial mats, should be revisited.

ACKNOWLEDGEMENTS

We thank Carolyn Colonero and Sharon Newman (MIT) for their help during sample preparation and analysis. Dr. Jochen Brocks is thanked for contributions to the discussion of biomarker composition. This work was supported by the 973 program (grant No. 2011CB808800, 2013CB955704), the 111 project (grant No. B08030), Natural Science Foundation of China (grant No. 41472170) and the fundamental research funds for the central universities, China University of Geosciences (CUG 130406 and CUG 120117). Research at MIT was supported by awards (NNA13AA90A) from the NASA Astrobiology Institute and the Simons Foundation. CH was supported by the Agouron Institute and by the Max Planck Society.

REFERENCES

Allen M. A., Neilan B. A., Burns B. P., Jahnke L. L. and Summons R. E. (2010) Lipid biomarkers in Hamelin Pool microbial mats and stromatolites. *Org. Geochem.* **41**, 1207–1218.

Allwood A. C., Walter M. R., Kamber B. S., Marshall C. P. and Burch I. W. (2006) Stromatolite reef from the Early Archaean era of Australia. *Nature* **441**, 714–718.

Bauersachs T., Schouten S., Compaore J., Wollenzien U., Stal L. J. and Sinninghe Damsté J. S. (2009) Nitrogen isotopic fractionation associated with growth on dinitrogen gas and nitrate by cyanobacteria. *Limnol. Oceanogr.* **54**, 1403–1411.

Beatty J. T., Overmann J., Lince M. T., Manske A. K., Lang A. S., Blankenship R. E., Van Dover C. L., Martinson T. A. and Plumley F. G. (2005) An obligately photosynthetic bacterial anaerobe from a deep-sea hydrothermal vent. *PNAS* **102**, 9306–9310.

Bian L. Z., Zhang S. C., Zhang B. M. and Wang D. R. (2005) Red algal fossils discovered from the Neoproterozoic Xiamaling oil shales, Xianhuayuan Town of Hebei Province. *Acta Micropalaeontolo. Sinica* **22**, 209–216.

Blumenberg M., Thiel V., Riegel W., Kah L. C. and Reitner J. (2012) Biomarkers of black shales formed by microbial mats, Late Mesoproterozoic (1.1 Ga) Taoudeni Basin, Mauritania. *Precambrian Res.* **196–197**, 113–127.

Bontognali T. R. R., Sessions A. L., Allwood A. C., Fischer W. W., Grotzinger J. P., Summons R. E. and Eiler J. M. (2012) Sulfur isotopes of organic matter preserved in 3.45-billion-year-old stromatolites reveal microbial metabolism. *PNAS* **109**, 15146–15151.

Boreham C. J., Crick I. H. and Powell T. G. (1988) Alternative calibration of the Methylphenanthrene index against vitrinite reflectance: Application to maturity measurements on oils and sediments. *Org. Geochem.* **12**, 289–294.

Brocks J. J. (2011) Millimeter-scale concentration gradients of hydrocarbons in Archean shales: Live-oil escape or fingerprint of contamination? *Geochim. Cosmochim. Acta* **75**, 3196–3213.

Brocks J. J. and Schaeffer P. (2008) Okenane, a biomarker for purple sulfur bacteria (Chromatiaceae), and other new carotenoid derivates from the 1640 Ma Barney Creek Formation. *Geochim. Cosmochim. Acta* **72**, 1396–1414.

Brocks J. J., Logan G. A., Buick R. and Summons R. E. (1999) Archean molecular fossils and the early rise of eukaryotes. *Science* **285**, 1033–1036.

Brocks J. J., Buick R., Logan G. A. and Summons R. E. (2003) Composition and syngeneity of molecular fossils from the 2.78 to 2.45 billion-year-old Mount Bruce Supergroup, Pilbara

Craton, Western Australia. *Geochim. Cosmochim. Acta* **67**, 4289–4319.

Brocks J. J., Love G. D., Summons R. E., Knoll A. H., Logan G. A. and Bowden S. A. (2005) Biomarker evidence for green and purple sulphur bacteria in a stratified Palaeoproterozoic sea. *Nature* **437**, 866–870.

Canfield D. E. (1998) A new model for Proterozoic ocean chemistry. *Nature* **396**, 450–453.

Cao C. Q., Love G. D., Hays L. E., Wang W., Shen S. Z. and Summons R. E. (2009) Biogeochemical evidence for euxinic oceans and ecological disturbance presaging the end-Permian mass extinction event. *Earth Planet. Sci. Lett.* **281**, 188–201.

Cavalier-Smith T. (2002) The neomuran origin of archaebacteria, the negibacterial root of the universal tree and bacterial megaclassification. *Int. J. Syst. Evol. Microbiol.* **52**, 7–76.

Chen J., Fu J., Sheng G., Liu D. and Zhang J. (1996) Diamondoid hydrocarbon ratios: Novel maturity indices for highly mature crude oils. *Org. Geochem.* **25**, 179–190.

Close H. G., Bovee R. and Pearson A. (2011) Inverse carbon isotope patterns of lipids and kerogen record heterogenous primary biomass. *Geobiology* **9**, 250–265.

de Leeuw J. W. and Largeau C. (1993) A review of macromolecular organic compounds that comprise living organisms and their role in kerogen, coal, and petroleum formation. In *Organic Geochemistry Topics in Geobiology*, vol. 11 (eds. M. Engel and S. Macko). Springer, US, pp. 23–72.

DeNiro M. J. and Epstein S. (1978) Influence of diet on the distribution of carbon isotopes in animals. *Geochim. Cosmochim. Acta* **42**, 495–506.

Derenne S., Robert F., Skrzypczak-Bonduelle A., Gourier D., Binet L. and Rouzaud J. N. (2008) Molecular evidence for life in the 3.5 billion year old Warrawoona chert. *Earth Planet. Sci. Lett.* **272**, 476–480.

Didyk B. M., Simoneit B. R. T., Brassell S. C. and Eglinton G. (1978) Organic geochemical indicators of paleoenvironmental conditions of sedimentation. *Nature* **272**, 216–222.

Doughty D. M., Hunter R. C., Summons R. E. and Newman D. K. (2009) 2-Methylhopanoids are maximally produced in akinetes of *Nostoc punctiforme*: Geobiological implications. *Geobiology* **7**, 1–9.

Dutkiewicz A., Volk H., Ridley J. and George S. (2003) Biomarkers, brines, and oil in the Mesoproterozoic, Roper Superbasin, Australia. *Geology* **31**, 981–984.

Dutkiewicz A., Volk H., George S. C., Ridley J. and Buick R. (2006) Biomarkers from Huronian oil-bearing fluid inclusions: An uncontaminated record of life before the Great Oxidation Event. *Geology* **34**, 437–440.

Dutta S., Bhattacharya S. and Raju S. V. (2013) Biomarker signatures from Neoproterozoic-Early Cambrian oil, western India. *Org. Geochem.* **56**, 68–80.

Eigenbrode J. L., Freeman K. H. and Summons R. E. (2008) Methylhopane biomarker hydrocarbons in Hamersley province sediments provide evidence for Neoarchean aerobiosis. *Earth Planet. Sci. Lett.* **273**, 323–331.

Farrimond P., Taylor A. and TelnÆs N. (1998) Biomarker maturity parameters: The role of generation and thermal degradation. *Org. Geochem.* **29**, 1181–1197.

French, K. L., Sepúlveda, J., Hays, L. E., Illing, C.J., Rocher, D., Zumberge, J. E. and Summons, R. E. (2013) Assessing the distribution of carotenoids through time using tandem mass spectrometry. In *The 26th IMOG*. pp. 161–162.

Gao L. Z., Zhang H. C., Shi X. Y., Song B., Wang Z. Q. and Liu Y. M. (2008) Mesoproterozoic age for Xiamaling Formation in North China Plate indicated by zircon SHRIMP dating. *Chinese Sci. Bull.* **53**, 2665–2671.

Goossens H., de Leeuw J. W., Schenck P. A. and Brassell S. C. (1984) Tocopherols as likely precursors of pristane in ancient sediments and crude oils. *Nature* **312**, 440–442.

Hallmann C., Schwark L. and Grice K. (2008) Community dynamics of anaerobic bacteria in deep petroleum reservoirs. *Nat. Geosci.* **1**, 588–591.

Hallmann C., Kelly A. E., Gupta N. S. and Summons R. E. (2011) Reconstructing deep time biology with molecular fossils. In *Quantifying the Evolution of Early Life: Topics in Geobiology*, vol. 36 (eds. M. Laflamme, J. D. Schiffbauer and S. Q. Dornbos). Springer, pp. 355–401.

Hatch J. R. and Leventhal J. S. (1992) Relationship between inferred redox potential of the depositional environment and geochemistry of the Upper Pennsylvanian (Missourian) Stark Shale Member of the Dennis Limestone, Wabaunsee County, Kansas, U.S.A. *Chem. Geol.* **99**, 65–82.

Huc A. Y. (1980) Origin and formation of organic matter in recent sediments and its relation to kerogen. In *Kerogen* (ed. B. Durand). Technip, Paris, pp. 445–474.

Hughes W. B., Holba A. G. and Dzou I. P. (1995) The ratios of dibenzothiophene to phenanthrene and pristane to phytane as indicators of depositional environment and lithology of petroleum source rocks. *Geochim. Cosmochim. Acta* **59**, 3581–3589.

Illing C. J., Hallmann C., Miller K. E., Summons R. E. and Strauss H. (2014) Airborne hydrocarbon contamination from laboratory atmospheres. *Org. Geochem.* **76**, 26–38.

Imbus S. W., Engel M. H., Elmore R. D. and Zumberge J. E. (1988) The origin, distribution and hydrocarbon generation potential of organic-rich facies in the Nonesuch formation, central North American Rift System: A regional study. *Org. Geochem.* **13**, 207–219.

Javaux E. J., Knoll A. H. and Walter M. R. (2001) Morphological and ecological complexity in early eukaryotic ecosystems. *Nature* **412**, 66–69.

Javaux E. J., Knoll A. H. and Walter M. R. (2004) TEM evidence for eukaryotic diversity in mid-Proterozoic oceans. *Geobiology* **2**, 121–132.

Javaux E. J., Marshall C. P. and Bekker A. (2010) Organic-walled microfossils in 3.2-billion-year-old shallow-marine siliciclastic deposits. *Nature* **463**, 934–939.

Jones B. and Manning D. A. C. (1994) Comparison of geochemical indices used for the interpretation of palaeoredox conditions in ancient mudstones. *Chem. Geol.* **111**, 111–129.

Köster J., Van Kaam-Peters H. M. E., Koopmans M. P., de Leeuw J. W. and Sinninghe Damsté J. S. (1997) Sulphurisation of homohopanoids: Effects on carbon number distribution, speciation, and 22S22R epimer ratios. *Geochim. Cosmochim. Acta* **61**, 2431–2452.

Kah L. C. and Bartley J. K. (2011) Protracted oxygenation of the Proterozoic biosphere. *Int. Geol. Rev.* **53**, 1424–1442.

Knoll A. H. (1992) The early evolution of eukaryotes: A geological perspective. *Science* **256**, 622–627.

Knoll A. H., Javaux E. J., Hewitt D. and Cohen P. (2006) Eukaryotic organisms in Proterozoic oceans. *Philos. Trans. R. Soc. B* **361**, 1023–1038.

Kuypers M. M. M., van Breugel Y., Schouten S., Erba E. and Sinninghe Damstée J. S. (2004) N_2-fixing cyanobacteria supplied nutrient N for Cretaceous oceanic anoxic events. *Geology* **32**, 853–856.

Li H. K., Lu S. N., Li H. M., Sun L. X., Xiang Z. Q., Geng J. Z. and Zhou H. Y. (2009) Zircon and beddeleyite U-Pb precision dating of basic rock sills intruding Xiamaling Formation, North China. *Geol. Bull. China* **28**, 1396–1404.

Liu Y. S., Zong K. Q., Kelemen P. B. and Gao S. (2008) Geochemistry and magmatic history of eclogites and ultramafic rocks from the Chinese continental scientific drill hole:

Subduction and ultrahigh-pressure metamorphism of lower crustal cumulates. *Chem. Geol.* **247**, 133–153.
Logan G. A., Hayes J. M., Hieshima G. B. and Summons R. E. (1995) Terminal Proterozoic reorganization of biogeochemical cycles. *Nature* **376**, 53–56.
Lu S. N., Zhao G. C., Wang H. C. and Hao G. J. (2008) Precambrian metamorphic basement and sedimentary cover of the North China Craton: A review. *Precambrian Res.* **160**, 77–93.
Luo G. M., Kump L. R., Wang Y. B., Tong J. N., Arthur M. A., Yang H., Huang J. H., Yin H. F. and Xie S. C. (2010) Isotopic evidence for an anomalously low oceanic sulphate concentration following end-Permian mass extinction. *Earth Planet. Sci. Lett.* **300**, 101–111.
Luo G. M., Wang Y. B., Grice K., Kershaw S., Algeo T. J., Ruan X., Yang H., Jia C. and Xie S. (2013) Microbial–algal community changes during the latest Permian ecological crisis: Evidence from lipid biomarkers at Cili, South China. *Global Planet. Change* **105**, 36–51.
Luo G. M., Junium C. K., Kump L. R., Huang J. H., Li C., Feng Q. L., Shi X. Y., Bai X. and Xie S. C. (2014) Shallow stratification prevailed for ~1700 to ~1300 Ma ocean: Evidence from organic carbon isotope composition in the North China Block. *Earth Planet. Sci. Lett.* **400**, 219–232.
Mckirdy D. M., Aldridge A. K. and Ypma P. J. M. (1981) A geochemical comparison of some crude oils from pre-Ordovician carbonate rocks. *Adv. Org. Geochem.*, 99–107.
Moldowan J. M., Sundararaman P. and Schoell M. (1986) Sensitivity of biomarker properties to depositional environment and/or source input in the Lower Toarcian of SW-Germany. *Org. Geochem.* **10**, 915–926.
Moldowan J. M., Fago F. J., Carlson R. M. K., Young D. C., an Duvne G., Clardy J., Schoell M., Pillinger C. T. and Watt D. S. (1991) Rearranged hopanes in sediments and petroleum. *Geochim. Cosmochim. Acta* **55**, 3333–3353.
Nicholson J. A. M., Stolz J. F. and Pierson B. K. (1987) Structure of a microbiol mat at Great Sippewissett Marsh, Cape Cod, Massachusetts. *FEMS Microbiol. Lett.* **45**, 343–364.
Ourisson G., Rohmer M. and Poralla K. (1987) Prokaryotic hopanoids and other polyterpenoid sterol surrogates. *Annu. Rev. Microbiol.* **41**, 301–333.
Overmann J. (2006) The Family Chlorobiaceae. In *The Prokaryotes* (eds. M. Dworkin, S. Falkow, E. Rosenberg, K. H. Schleifer and E. Stackebrandt). Springer, New York, pp. 359–378.
Pawlowska M. M., Butterfield N. J. and Brocks J. J. (2013) Lipid taphonomy in the Proterozoic and the effect of microbial mats on biomarker preservation. *Geology* **41**, 103–106.
Peakman T. M. and Maxwell J. R. (1988) Early diagenetic pathways of steroid alkenes. *Org. Geochem.* **13**, 583–592.
Pearson A., Page S. R. F., Jorgenson T. L., Fischer W. W. and Higgins M. B. (2007) Novel hopanoid cyclases from the environment. *Environ. Microbiol.* **9**, 2175–2188.
Peters K. E. and Moldowan J. M. (1991) Effects of source, thermal maturity, and biodegradation on the distribution and isomerization of homohopanes in petroleum. *Org. Geochem.* **17**, 47–61.
Peters K. E., Walters C. C. and Moldowan J. M. (2005) *The Biomarker Guide: Biomarkers and Isotopes in the Environment and Human History*. Cambridge University Press, Cambridge.
Philp R. P. and Gilbert T. D. (1986) Biomarker distributions in Australian oils predominantly derived from terrigenous source material. *Org. Geochem.* **10**, 73–84.
Planavsky N. J., McGoldrick P., Scott C. T., Li C., Reinhard C. T., Kelly A. E., Chu X., Bekker A., Love G. D. and Lyons T. W. (2011) Widespread iron-rich conditions in the mid-Proterozoic ocean. *Nature* **477**, 448–451.
Poulton S. W., Fralick P. W. and Canfield D. E. (2010) Spational variability in oceanic redox structure 1.8 billion years ago. *Nat. Geosci.* **3**, 486–490.
Pratt L. M., Hieshima G. B. and Summons R. E. (1991) Sterane and triterpane biomarkers in the Precambrian Nonesuch Formation, North American Midcontinent Rift. *Geochim. Cosmochim. Acta* **55**, 911–916.
Qiao X. F., Gao L. Z. and Zhang C. H. (2007) New idea of the Meso- and Neoproterozoic chronostratigraphic chart and tectonic environment in Sino-Korean Plate. *Geol. Bull. China* **26**, 503–509.
Radke M. and Welte D. H. (1981) The methylphenanthrene index (MPI): A maturity parameter based on aromatic hydrocarbons. *Adv. Org. Geochem.* **19**, 504–512.
Rasmussen B., Fletcher I. R., Brocks J. J. and Kilburn M. R. (2008) Reassessing the first appearance of eukaryotes and cyanobacteria. *Nature* **455**, 1101–1105.
Ricci J. N., Coleman M. L., Welander P. V., Sessions A. L., Summons R. E., Spear J. R. and Newman D. K. (2014) Diverse capacity for 2-methylhopanoid production correlates with a specific ecological niche. *ISME J.* **8**, 675–684.
Rohmer M., Bouvier-Nave P. and Ourisson G. (1984) Distribution of hopanoid triterpenes in prokaryotes. *J. Gen. Microbiol.* **130**, 1137–1150.
Rohmer M. and Ourisson G. (1986) Unsaturated bacteriohopanepolyols from *Acetobacter aceti* ssp. *xylinum*. *J. Chem. Res.* **10**, 356–357.
Rohrssen M., Love G. D., Fischer W., Finnegan S. and Fike D. A. (2013) Lipid biomarkers record fundamental changes in the microbial community structure of tropical seas during the Late Ordovician Hirnantian glaciation. *Geology* **41**, 127–130.
Rubinstein I., Sieskind O. and Albrecht P. (1975) Rearranged steranes in a shale: Occurrence and simulated formation. *J. Chem. Soc., Perkin Trans. I*, 1833–1836.
Rullkötter J. and Marzi R. (1988) Natural and artificial maturation of biological markers in a Toarcian shale from northern Germany. *Org. Geochem.* **13**, 639–645.
Rullkötter J., Spiro B. and Nissenbaum A. (1985) Biological marker characteristics of oils and asphalts from carbonate source rocks in a rapidly subsiding graben, Dead Sea, Israel. *Geochim. Cosmochim. Acta* **49**, 1357–1370.
Sáenz J. P., Eglinton T. I. and Summons R. E. (2011) Abundance and structural diversity of bacteriohopanepolyols in suspended particulate matter along a river to ocean transect. *Org. Geochem.* **42**, 774–780.
Sáenz J. P., Waterbury J. B., Eglinton T. I. and Summons R. E. (2012) Hopanoids in marine cyanobacteria: Probing their phylogenetic distribution and biological role. *Geobiology* **10**, 311–319.
Scott C., Lyons T. W., Bekker A., Shen Y. A., Poulton S. W., Chu X. L. and Anbar A. D. (2008) Tracing the stepwise oxygenation of the Proterozoic ocean. *Nature* **452**, 456–460.
Shen Y. A., Buick R. and Canfield D. E. (2001) Isotopic evidence for microbial sulphate reduction in the early Archaean era. *Nature* **410**, 77–81.
Shen Y. A., Knoll A. H. and Walter M. R. (2003) Evidence for low sulphate and anoxia in a mid-Proterozoic marine basin. *Nature* **423**, 632–635.
Sherman L. S., Waldbauer J. R. and Summons R. E. (2007) Methods for biomarker analysis of highly mature Precambrian rocks. *Org. Geochem.* **38**, 1987–2000.
Shiea J., Brassell S. C. and Ward D. M. (1990) Mid-chain branched mono- and dimethyl alkanes in hot spring cyanobacterial mats: A direct biogenic source for branched alkanes in ancient sediments? *Org. Geochem.* **15**, 223–231.
Sigman D. M., Karsh K. L. and Casciotti K. L. (2009) Nitrogen isotopes in the ocean. In *Encyclopedia of Ocean Sciences* (eds. J.

H. Steele, S. A. Thorpe and K. K. Turekian). Academic Press, London, pp. 40–54.

Sieskind O., Joly G. and Albrecht P. (1979) Simulation of the geochemical transformation of sterols: Superacid effects of clay minerals. *Geochim. Cosmochim. Acta* **43**, 1675–1679.

Sinninghe Damsté J. S., Kok M. D., Köster J. and Schouten S. (1998) Sulfurized carbohydrates: An important sedimentary sink for organic carbon? *Earth Planet. Sci. Lett.* **164**, 7–13.

Smith M. and Bend S. (2004) Geochemical analysis and familial association of Red River and Winnipeg reservoired oils of the Williston Basin, Canada. *Org. Geochem.* **35**, 443–452.

Su W. B., Zhang S. H., Huff W. D., Ettensohn F. R., Chen X. Y., Yang H. M., Han Y. G., Song B. and Santosh M. (2008) SHRIMP U–Pb ages of K-bentonite beds in the Xiamaling Formation: Implications for revised subdivision of the Meso- to Neoproterozoic history of the North China Craton. *Gondwana Res.* **14**, 543–553.

Su W. B., Li H. K., Huff W. D., Ettensohn F. R., Zhang S. H., Zhou H. Y. and Wan Y. S. (2010) SHRIMP U–Pb dating for a K-bentonite bed in the Tieling Formation, North China. *Chinese Sci. Bull.* **55**, 3312–3323.

Summons R. E. and Lincoln S. A. (2012) Biomarkers: Informative molecules for studies in geobiology. In *Fundamentals of Geobiology* (eds. A. H. Knoll, D. E. Canfield and K. O. Konhauser). Blackwell Publishing, Ltd, pp. 269–296.

Summons R. E. and Powell T. G. (1987) Chlorobiaceae in Palaeozoic sea revealed by biological markers, isotopes and geology. *Nature* **319**, 763–765.

Summons R. E. and Walter M. R. (1990) Molecular fossils and microfossils of prokaryotes and protists from proterozoic sediments. *Am. J. Sci.* **290-A**, 212–244.

Summons R. E., Brassell S. C., Eglinton G., Evans E., Horodyski R. J., Robinson N. and Ward D. M. (1988a) Distinctive hydrocarbon biomarkers from fossiliferous sediment of the Late Proterozoic Walcott Member, Chuar Group, Grand Canyon, Arizona. *Geochim. Cosmochim. Acta* **52**, 2625–2637.

Summons R. E., Powell T. G. and Boreham C. J. (1988b) Petroleum geology and geochemistry of the Middle Proterozoic McArthur Basin, northern Australia: III. Composition of extractable hydrocarbons. *Geochim. Cosmochim. Acta* **52**, 1747–1763.

Summons R. E., Jahnk e. L. L. and Roksandic Z. (1994) Carbon isotopic fractionation in lipids from methanotrophic bacteria: Relevance for interpretation of the geochemical record of biomarkers. *Geochim. Cosmochim. Acta* **58**, 2853–2863.

Summons R. E., Jahnke L. L., Hope J. M. and Logan G. A. (1999) 2-Methylhopanoids as biomarkers for cyanobacterial oxygenic photosynthesis. *Nature* **400**, 554–557.

Talbot H. M., Rohmer M. and Farrimond P. (2007) Structural characterisation of unsaturated bacterial hopanoids by atmospheric pressure chemical ionisation liquid chromatography/ion trap mass spectrometry. *Rapid Commun. Mass Spectrom.* **21**, 1613–1622.

Talbot H. M., Summons R. E., Jahnke L. L., Cockell C. S., Rohmer M. and Farrimond P. (2008) Cyanobacterial bacteriohopanepolyol signatures from cultures and natural environmental settings. *Org. Geochem.* **39**, 232–263.

Tamiaki H., Shibata R. and Mizoguchi T. (2007) The 17-propionate function of (bacterio)chlorophylls: Biological implication of their long esterifying chains in photosynthetic systems. *Photochem. Photobiol.* **83**, 152–162.

Telnaes N., Isaksen G. H. and Farrimond P. (1992) Unusual triterpane distributions in lacustrine oils. *Org. Geochem.* **18**, 785–789.

ten Haven H. L., de Leeuw J. W., Rulkotter J. and Sinninghe Damsté J. S. (1987) Restricted utility of the pristane/phytane ratio as a palaeoenvironmental indicator. *Nature* **330**, 641–643.

Ueno Y., Ono S., Rumble D. and Maruyama S. (2008) Quadruple sulfur isotope analysis of ca. 3.5 Ga Dresser Formation: New evidence for microbial sulfate reduction in the early Archean. *Geochim. Cosmochim. Acta* **72**, 5675–5691.

van Kaam-Peters H. M. E., Köster J., van der Gaast S. J., Dekker M., de Leeuw J. W. and Sinninghe Damsté J. S. (1998) The effect of clay minerals on diasterane/sterane ratios. *Geochim. Cosmochim. Acta* **62**, 2923–2929.

Volkman J. K. (1983) Biodegradation of aromatic hydrocarbons in crude oils from the Barrow sub-basin of Western Australia. *Org. Geochem.* **6**, 619–632.

Waldbauer J. R., Sherman L. S., Sumner D. Y. and Summons R. E. (2009) Late Archean molecular fossils from the Transvaal Supergroup record the antiquity of microbial diversity and aerobiosis. *Precambrian Res.* **169**, 28–47.

Wang L. F. and Li B. H. (1993) Sedimentary sequences and source beds in the Xiamaling formation in Northwestern Hebei. *Lithofacies Palaeogeogr.* **13**, 38–45.

Wang T. G. and Simoneit B. R. T. (1995) Tricyclic terpanes in Precambrian bituminous sandstone from the eastern Yanshan region, North China. *Chem. Geol.* **120**, 155–170.

Welander P. V. and Summons R. E. (2012) Discovery, taxonomic distribution, and phenotypic characterization of a gene required for 3-methylhopanoid production. *PNAS* **109**, 12905–12910.

Welander P. V., Coleman M. L., Sessions A. L., Summons R. E. and Newman D. K. (2010) Identification of a methylase required for 2-methylhopanoid production and implications for the interpretation of sedimentary hopanes. *PNAS* **107**, 8537–8542.

Welander P. V., Doughty D. M., Wu C. H., Mehay S., Summons R. E. and Newman D. K. (2012) Identification and characterization of *Rhodopseudomonas palustris* TIE-1 hopanoid biosynthesis mutants. *Geobiology* **10**, 163–177.

Werne J. P., Lyons T. W., Hollander D. J., Schouten S., Hopmans E. C. and Sinninghe Damsté J. S. (2008) Investigating pathways of diagenetic organic matter sulfurization using compound-specific sulfur isotope analysis. *Geochim. Cosmochim. Acta* **72**, 3489–3502.

Williford K. H., Grice K., Logan G. A., Chen J. and Huston D. (2011) The molecular and isotopic effects of hydrothermal alteration of organic matter in the Paleoproterozoic McArthur River Pb/Zn/Ag ore deposit. *Earth Planet. Sci. Lett.* **301**, 382–392.

Xie S. C., Pancost R. D., Yin H. F., Wang H. M. and Evershed R. P. (2005) Two episodes of microbial change coupled with Permo/Triassic faunal mass extinction. *Nature* **434**, 494–497.

Xie L. J., Sun Y. G., Yang Z. W., Chen J. P., Jiang A. Z., Zhang Y. D. and Deng C. P. (2013) Evaluation of hydrocarbon generation of the Xiamaling Formation shale in Zhangjiakou and its significance to petroleum geology in North China. *Sci. China Ser. D* **56**, 444–452.

Yoon H. S., Hackett J. D., Ciniglia C., Pinto G. and Bhattacharya D. (2004) A Molecular Timeline for the Origin of Photosynthetic Eukaryotes. *Mol. Biol. Evol.* **21**, 809–818.

Zhu Y., Hao F., Zou H., Cai X. and Luo Y. (2007) Jurassic oils in the central Sichuan basin, southwest China: Unusual biomarker distribution and possible origin. *Org. Geochem.* **38**, 1884–1896.

Zundel M. and Rohmer M. (1985) Prokaryotic triterpenoids. 3. The biosynthesis of 2b-methylhopanoids and 3b-methylhopanoids of *Methylobacterium organophilum* and *Acetobacter pasteurianus* ssp. *pasteurianus*. *Eur. J. Biochem.* **150**, 35–39.

Associate editor: Thomas Wagner